ADVANCED MATERIALS INTERFACES
Open Access
www.advmatinterfaces.de

Check for updates

Chemical–Mechanical Polishing of 4H Silicon Carbide Wafers

Wantang Wang, Xuesong Lu, Xinke Wu, Yiqiang Zhang, Rong Wang, Deren Yang, and Xiaodong Pi**

4H silicon carbide (4H-SiC) holds great promise for high-power and high-frequency electronics, in which high-quality 4H-SiC wafers with both global and local planarization are cornerstones. Chemical–mechanical polishing (CMP) is the key processing technology in the planarization of 4H-SiC wafers. Enhancing the performance of CMP is critical to improving the surface quality and reducing the processing cost of 4H-SiC wafers. In this review, the superior properties of 4H-SiC and the processing of 4H-SiC wafers are introduced. The development of CMP with chemical, mechanical, and chemical–mechanical synergistic approaches to improve the performance of CMP is systematically reviewed. The basic principle and processing system of each improvement approach are presented. By comparing the material removal rate of CMP and the surface roughness of CMP-treated 4H-SiC wafers, the prospect on the chemical, mechanical, and chemical–mechanical synergistic improvement approaches is finally provided.

W. Wang, X. Wu
College of Electrical Engineering
Zhejiang University
Hangzhou, Zhejiang 310027, P. R. China
W. Wang, X. Lu, R. Wang, D. Yang, X. Pi
State Key Laboratory of Silicon and Advanced Semiconductor Materials
& School of Materials Science and Engineering
Zhejiang University
Hangzhou, Zhejiang 310027, P. R. China
E-mail: rong_wang@zju.edu.cn; xdpi@zju.edu.cn
W. Wang, X. Lu, X. Wu, R. Wang, D. Yang, X. Pi
Institute of Advanced Semiconductors & Zhejiang Provincial
Key Laboratory of Power Semiconductor Materials and Devices
ZJU-Hangzhou Global Scientific and Technological Innovation Center
Zhejiang University
No. 733 Jianshe San Road, Hangzhou, Zhejiang 311200, P. R. China
Y. Zhang
School of Materials Science and Engineering & College of Chemistry
Zhengzhou University
Zhengzhou, Henan 450001, P. R. China

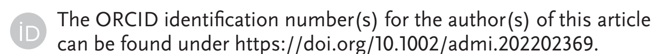
The ORCID identification number(s) for the author(s) of this article can be found under https://doi.org/10.1002/admi.202202369.

© 2023 The Authors. Advanced Materials Interfaces published by Wiley-VCH GmbH. This is an open access article under the terms of the Creative Commons Attribution License, which permits use, distribution and reproduction in any medium, provided the original work is properly cited.

DOI: 10.1002/admi.202202369

1. Introduction

4H silicon carbide (4H-SiC) is emerging as a dominant semiconductor material to enable the ever-increasing deployment of high-power, high-frequency, high-temperature and radiation-resistant devices.[1,2] Compared with silicon (Si)-based the high-power devices based on 4H-SiC have the advantages of higher power density, lower power consumption, and smaller size.[3] As shown in **Figure 1**, the devices using 4H-SiC have been successfully utilized in a series of fields such as electric vehicles, railways, uninterruptible power supplies (UPS), high-voltage grids, and 5G communications.[4] For example, the power-conversion efficiency of the G2020 series 4H-SiC-based UPS developed by Toshiba has reached 98.2%.[1] Toyota has replaced Si-based PIN diodes with 4H-SiC-based Schottky-barrier diodes in the DC converters of hybrid electric vehicles, leading to 30% reduction of energy loss and 0.5% increase of conversion efficiency.[5] Mitsubishi Electric Corporation has equipped a 4H-SiC power module in the train traction inverter of the N700S Shinkansen subway, enabling the switching loss and volume of the system to be reduced by 55% and 40–65%, respectively.[6] The promising applications of 4H-SiC have boosted the requirements for high-quality 4H-SiC wafers. Since the surface quality of 4H-SiC wafers significantly affects the quality of epitaxial 4H-SiC (homoepitaxy) or GaN (heteroepitaxy) and thus the quality of final devices, the processing of the surface of 4H-SiC wafers is crucial to the success of 4H-SiC in semiconductor industry.[7]

Chemical–mechanical polishing (CMP) has been developed as a state-of-the-art technology to achieve global planarization of the surface of 4H-SiC wafers.[8] During CMP, the surface of a 4H-SiC wafer undergoes cycles of chemical oxidation and mechanical removal under the interaction among the 4H-SiC wafer, polishing slurry, and polishing pad.[9] Given the high hardness and strong chemical inertness of 4H-SiC, the CMP of 4H-SiC wafers faces the challenges of long processing time, high cost, and low technical flexibility.[10,11] In order to improve the surface quality and processing efficiency of 4H-SiC wafers, researchers have been investigating various approaches.

In this review, we discuss recent progress on the CMP of 4H-SiC wafers after a brief overview of the basic properties of 4H-SiC. Chemical, mechanical, and chemical–mechanical

21967350, 2023, 13, Downloaded from https://onlinelibrary.wiley.com/doi/10.1002/admi.202202369 by Xiamen University, Wiley Online Library on [11/04/2024]. See the Terms and Conditions (https://onlinelibrary.wiley.com/terms-and-conditions) on Wiley Online Library for rules of use; OA articles are governed by the applicable Creative Commons License

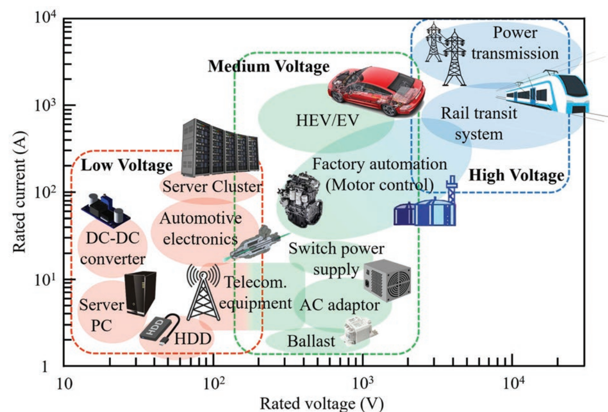

Figure 1. Major application fileds of the electronic devices based on 4H-SiC.

synergistic approaches for the efficiency improvement of CMP are highlighted. By discussing the advantages and disadvantages of the efficiency-improvement approaches, we analyze the challenges of using these approaches in industry. Finally, prospects on the development of the CMP of 4H-SiC wafers are presented.

2. Properties and Manufacturing of 4H-SiC Wafers

2.1. Properties of SiC

The bonding between Si and C is shown in **Figure 2**a. The bond length and binding energy of Si—C are ≈1.89 Å and ≈289 kJ mol^{-1}, respectively. They give rise to the extremely high hardness and strong chemical stability of SiC.[12] SiC has more than 200 homogeneous polymorphs, of which 3C-, 4H-, and 6H-SiC are rather common.[13] The structures of 3C-, 4H-, and 6H-SiC are schematically shown in Figure 2b. The letters A, B, and C denote sites occupied by Si—C bilayers in a hexagonal close-packed structure. The stacking sequences of Si—C bilayers of 3C-, 4H-, and 6H-SiC are ABC, ABCB, and ABCACB, respectively. Figure 2c displays crystal directions and planes of hexagonal 4H-SiC.[14] The planes with the direction of [0001] and [000$\bar{1}$] are often called the Si face and C face, respectively. The (11$\bar{2}$0) plane and (1$\bar{1}$00) plane are often denoted as the ***a*** face and ***m*** face, respectively. For 4H-SiC, the electron mobility along the *c*-axis is higher than that perpendicular to the *c*-axis. Furthermore, the step-flow growth mode and the p-type doping are both enhanced on the Si face of 4H-SiC substrates.[15,16] Therefore, the homoepitaxy of the 4H-SiC substrate is often grown on the Si-face. In view of this, the CMP technologies of the Si face of 4H-SiC wafers have attracted great attention.

Given the same bonding between Si and C, 3C-, 4H-, and 6H-SiC have similar mechanical and chemical properties. However, due to the different stacking sequences of Si—C bilayers, the electrical properties of 3C-, 4H-, and 6H-SiC are different from each other.[17] As shown in **Figure 3**, the critical electric field, bandgap energy, saturated electron velocity and electron mobility of 4H-SiC all prevail over those of 3C- and 6H-SiC, which makes 4H-SiC being the ideal polymorph of SiC for the applications of high-power, high-frequency, and high-temperature electronics.[18] Therefore, we focus on the improvement of the CMP of 4H-SiC in this review. It should be noted that early work was mainly related to the CMP of 6H-SiC. Because of the similar mechanical and chemical properties of 4H- and 6H-SiC, the mechanical and chemical improvements for the CMP of 6H-SiC wafers are conducive to the improvements of the CMP of 4H-SiC wafers.

2.2. Manufacturing of 4H-SiC Wafers

As shown in **Figure 4**, the processing procedure of a 4H-SiC wafer mainly includes wire sawing, edge rounding, grinding, lapping, and CMP.[7,19] Firstly, a 4H-SiC boule is sliced into wafers during multi-wire sawing. Each 4H-SiC wafer is then mounted on a grinding chuck. A profile rounding wheel rounds the wafer edge according to the product's specifications. Grinding is subsequently carried out to rapidly reduce the thickness of the wafer. The wafer further undergoes a series of lapping processes to increase the parallelism of the surfaces and remove surface/sub-surface damage induced by the wire-sawing. Finally, CMP is used to improve the flatness and achieve an atomically smooth surface of the wafer.

The CMP process is a crucial step to control the surface quality of 4H-SiC wafers, while other steps mainly aim to remove the wire-sawing-induced damages and rapidly reduce

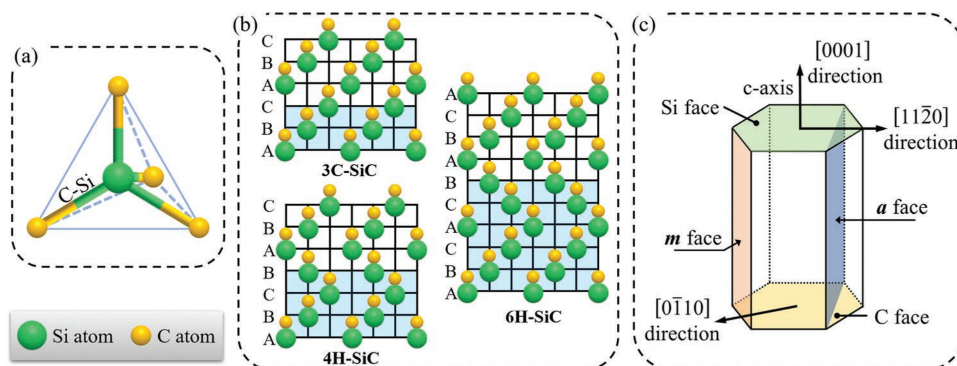

Figure 2. Schematic diagrams of a) tetrahedron structure formed by Si—C bonds, b) stacking sequence of Si—C bilayers in 3C-, 4H-, and 6H-SiC, and c) major crystal faces in hexagonal SiC.

 © 2023 The Authors. Advanced Materials Interfaces published by Wiley-VCH GmbH

21967350, 2023, 13, Downloaded from https://onlinelibrary.wiley.com/doi/10.1002/admi.202202369 by Xiamen University, Wiley Online Library on [11/04/2024]. See the Terms and Conditions (https://onlinelibrary.wiley.com/terms-and-conditions) on Wiley Online Library for rules of use; OA articles are governed by the applicable Creative Commons License

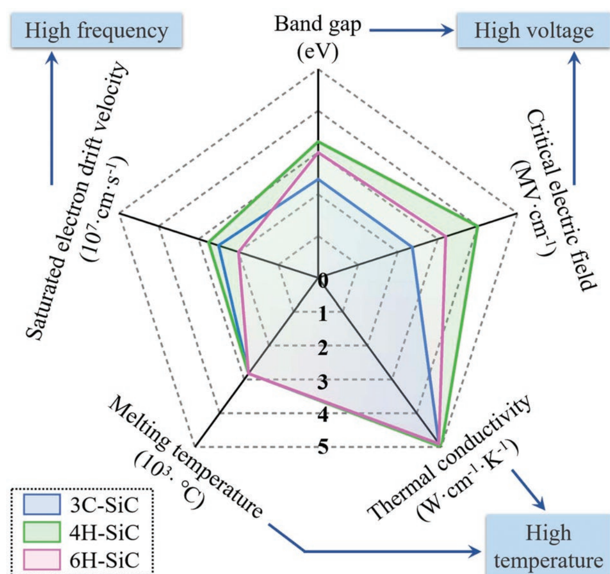

Figure 3. Comparison of physical properties and electronic properties of 3C-, 4H-, and 6H-SiC.

the thickness of 4H SiC wafers.[20] The cost of CMP accounts for 30–40% of the total processing cost of 4H-SiC wafers. The CMP of the Si face or C face of 4H-SiC wafers takes 3–5 hours. Both the cost and efficiency of the CMP of 4H-SiC wafers deserve further optimization although existing CMP approaches can be employed to produce qualified 4H-SiC wafers.[21]

3. Status and Challenges of the Chemical–Mechanical Polishing (CMP) of 4H-SiC Wafers

3.1. Traditional CMP Methods

CMP appeared in the mid-20th century, which had attracted great attention owing to its capability of planarizing both glass and metal.[22] When IBM corporation first introduced CMP to the manufacturing of integrated circuits in 1988, CMP began to be widely used in the processing of semiconductor wafers because both the global and local planarization can be achieved simultaneously.[23] As shown in **Figure 5**, a CMP system mainly consists of three parts: the polishing slurry, the polishing pad, and the polishing machine containing components such as the polishing head and polishing plate.[24] In a typical CMP process, a wafer is bonded to the bottom of a polishing head. The polishing slurry with specific functions is continuously dripped to the surface of the polishing pad. The wafer, polishing slurry, and polishing pad are in close contact under certain pressure and rotated with the polishing head and polishing plate. During the relative motion, the surface of the wafer and the polishing slurry chemically react. The reaction product is removed by the mechanical interaction among abrasives in the polishing slurry, the polishing pad and the wafer. The global and local planarization of the wafer is ultimately realized by the cycling of the chemical reaction and mechanical removal processes.

In 1997, CMP was first employed in the planarization of SiC wafers.[25] Diamond particles and SiO_2 particles were used as the abrasives of the mechanical polishing and CMP of 4H-SiC wafers, which yielded that the material removal rate (MRR) of the mechanical polishing and CMP were 2–2.25 μm h^{-1} and lower than 200 nm h^{-1}, respectively. The surface roughness after mechanical polishing and CMP were 70 and 0.5 nm, respectively. Processing parameters such as the rotation speed, pressure, and temperature are key factors affecting the CMP performance of 4H-SiC wafers. It was found that the maximum MRR of 250 nm h^{-1} for CMP could be realized at the temperature of 23 °C, the pressure of 5 psi, the polishing head rotation speed of 180 rpm, and the pH of 9.9.[26] With an alkaline-based polishing slurry, the MRR of 4H-SiC reached 0.1–0.5 μm h^{-1}. The surface roughness of 4H-SiC was less than 5 nm.[27] It is observed that the MRR of 6H-SiC increased by 20% after adding 0.6 wt% KOH to the slurry.[28] A series of more in-depth analyses shed light on the formation mechanism of atomic step-terrace structure on the surface of 6H- and 4H-SiC wafers after CMP.[11,29–31] As shown in **Figure 6**a, when the surface roughness of a 4H-SiC wafer is extremely low (*Ra* [the arithmetic mean deviation of contours] < 0.06 nm), the surface of the 4H-SiC wafer features a step-terrace structure. The atomic

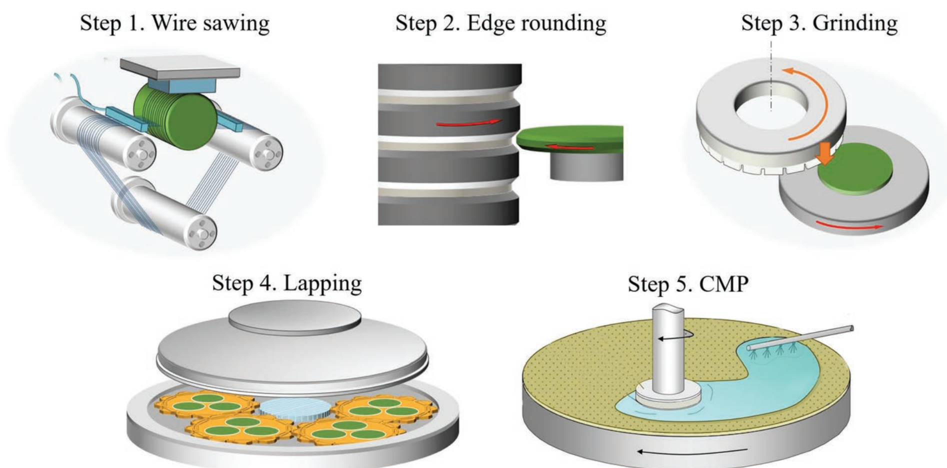

Figure 4. Schematic diagram of typical manufacturing procedures of 4H-SiC wafers, including wire sawing, edge rounding, grinding, lapping, and CMP.

© 2023 The Authors. Advanced Materials Interfaces published by Wiley-VCH GmbH

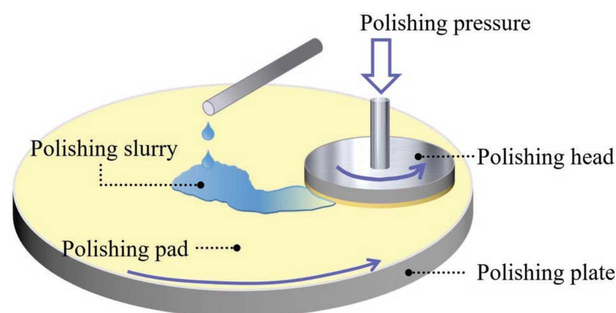

Figure 5. Schematic diagram of a typical CMP system, including polishing head, polishing plate, polishing slurry, and polishing pad. During CMP process, the 4H-SiC wafer, polishing slurry, and polishing pad are in close contact under certain pressure and rotated with the polishing head and polishing plate.

force microscope (AFM) measurement in Figure 6b shows that the step height of h about 0.25 nm. Combined with the crystal structure model of 4H-SiC in Figure 6c, the step height (*h*) of a bimolecular layer of 4H-SiC is calculated from the lattice parameters to be 0.25 nm. Therefore, the mutual corroboration of experiments and theory indicates that CMP can realize the processing requirements of atomically smooth surface of 4H-SiC wafer.

The removal mechanism of the CMP of 4H-SiC wafers is shown in **Figure 7**.[32] The oxidant in the polishing slurry firstly oxidizes 4H-SiC, forming the transition oxidation state of Si—C—O on the surface of 4H-SiC. The oxide has a lower hardness than that of 4H-SiC, which ensures that it can be removed by the abrasives in the slurry through mechanical effect. Based on the cycling of the oxidation and mechanical removal, the planarization of a 4H-SiC wafer is realized (Figure 7).[30] It has been proposed that the oxidation is the rate-limiting step in the whole CMP process.[33] H_2O_2 and colloidal silica were initially used as the oxidant and abrasive, respectively. A low MRR (<200 nm h^{-1}) was obtained. Before CMP, the depth of the surface damage of a 4H-SiC wafer is usually 2–5 µm.[34] The low MRR means that the CMP step requires significant processing time and costs.

Researchers have started improving the efficiency of CMP by accelerating oxidation. Potassium permanganate ($KMnO_4$) is of considerable interest because of its excellent capability of oxidation. By using $KMnO_4$ as the oxidant and colloidal silica as the abrasives, the MRR of 185 nm h^{-1} and *Ra* of 0.254 nm for the CMP of 6H-SiC were obtained.[35] The MRR might be further

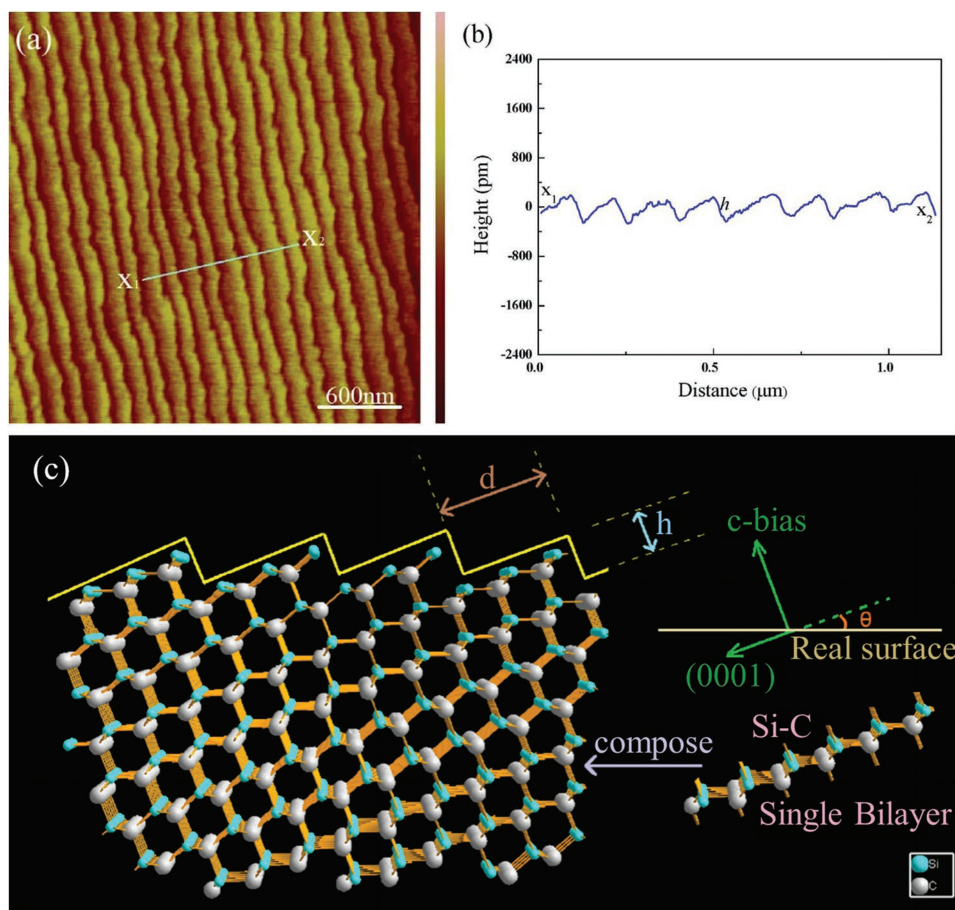

Figure 6. a) AFM image showing the atomic step structure on the surface of 4H-SiC wafers, b) dimension of the atomic steps measured from X_1 to X_2 labeled in (a), and c) formation mechanism of atomic step structure on the surface of 4H-SiC, where *d* and *h* denote the width and height of the steps. Reproduced with permission.[11] Copyright 2014, Elsevier.

 © 2023 The Authors. Advanced Materials Interfaces published by Wiley-VCH GmbH

21967350, 2023, 13, Downloaded from https://onlinelibrary.wiley.com/doi/10.1002/admi.202202369 by Xiamen University, Wiley Online Library on [11/04/2024]. See the Terms and Conditions (https://onlinelibrary.wiley.com/terms-and-conditions) on Wiley Online Library for rules of use; OA articles are governed by the applicable Creative Commons License

21967350, 2023, 13, Downloaded from https://onlinelibrary.wiley.com/doi/10.1002/admi.202202369 by Xiamen University, Wiley Online Library on [11/04/2024]. See the Terms and Conditions (https://onlinelibrary.wiley.com/terms-and-conditions) on Wiley Online Library for rules of use; OA articles are governed by the applicable Creative Commons License

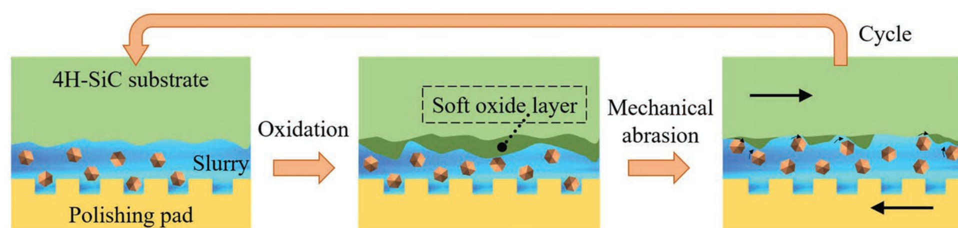

Figure 7. Schematic diagram of CMP principle of 4H-SiC wafer. The three diagrams are unfolded sequentially with the direction of the arrows, representing the dynamic process of the formation and removal of the oxide layer. Among them, the green polygon represents the 4H-SiC wafer, the blue polygon represents the polishing slurry, and the brown hexagon represents the abrasive grains in the polishing liquid, and the yellow polygon represents the polishing pad. Reproduced with permission.[32] Copyright 2021, Elsevier.

increased to 308 nm h^{-1} in a strong acid environment.[36] However, insufficient mechanical action limited the timely removal of the oxide layer and thus the efficiency of CMP in these studies. It was found that increasing the size of SiO_2 abrasives could increase the MRR. But the surface quality was scarified.[29] Therefore, the CMP efficiency must be enhanced by balancing the chemical oxidation and mechanical removal.

3.2. Chemical-Improvement Approaches

3.2.1. Fenton-Like-Reaction

The standard reduction potential of hydroxyl radicals ($^{\bullet}OH$) and H_2O_2 are 1.90–2.80 V and 1.77 V, respectively.[37] Therefore, the hydroxyl radicals ($^{\bullet}OH$) generated by Fenton reagents are more oxidizing than H_2O_2, which can be adopted to accelerate the oxidation process during the CMP of 4H-SiC. Taking the Fe catalyst as an example, the Fenton reaction can be described as:

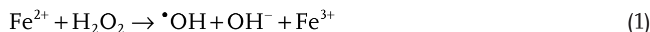

$$Fe^{2+} + H_2O_2 \rightarrow {}^{\bullet}OH + OH^- + Fe^{3+} \quad (1)$$

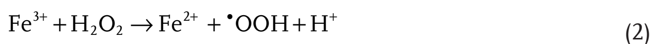

$$Fe^{3+} + H_2O_2 \rightarrow Fe^{2+} + {}^{\bullet}OOH + H^+ \quad (2)$$

It is clear that the main factors affecting the Fenton reaction are the pH value, Fe^{2+} dosage, and the concentration of H_2O_2. Some researchers used the rotation friction of a Fe rod to introduce Fe^{2+} to the CMP of 4H-SiC wafers, increasing the removal volume to ≈2300 μm^3 h^{-1}.[38] The overall removal mechanism of the CMP adopting Fenton-like reaction is:

$$2H_2O_2 \rightarrow 2H_2O + O_2 \quad (3)$$

$$H_2O_2 \rightarrow 2{}^{\bullet}OH \quad (4)$$

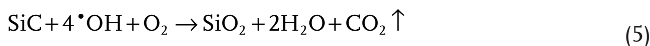

$$SiC + 4{}^{\bullet}OH + O_2 \rightarrow SiO_2 + 2H_2O + CO_2\uparrow \quad (5)$$

$$SiO_2 + 2OH^- \rightarrow SiO_3^{2-} + H_2O \quad (6)$$

It has been found that the catalytic effect of Fe-based catalysts decreases in the order of Fe_3O_4, FeO, Fe, and Fe_2O_3.[39–42] More significantly, the concentration ratio of Fe^{2+} and H_2O_2 plays an important role in the effective concentration of $^{\bullet}OH$ in the slurry. High Fe^{2+} concentration leads to flocculent precipitates in the slurry of CMP under acidic conditions, while high H_2O_2 concentration leads to partial quenching of the concentration of $^{\bullet}OH$.

The performance of CMP improved by the Fenton-like reaction is limited by the pH value of the slurry. Both the catalytic efficiency of the Fenton reaction and the stability of the slurry are highly dependent on the pH environment. When the pH value of slurry is higher than 3, Fe^{2+} converts to Fe $(OH)_3$ precipitation, resulting in a decrease in the efficiency of the Fenton reaction. The Fenton reaction experiments in these studies were mainly carried out under strong acid conditions (pH < 3), thus avoiding the problem of Fe $(OH)_3$ precipitation. On the other hand, the abrasives in the slurry tend to agglomerate under acid conditions, which degrades the performance of mechanical removal and thus the surface quality of 4H-SiC wafers. That is to say, when the pH value of the slurry is in the range of 3–7, the slurry suffers from both problems of Fe $(OH)_3$ precipitation and abrasive agglomeration. This agglomeration problem may not be severe at the stage of experiment research, because the execution time of a single CMP experiment is usually 1 h and the polishing slurry is not recycled. However, in the mass production of 4H-SiC wafers, the execution time of a single CMP process is 3–5 h, and the polishing slurry circulation time is usually more than 10 h. Therefore, when the technology moves from the lab to the fab, the agglomeration of colloidal silica will become a growing problem that cannot be ignored under strong acid conditions.

3.2.2. Special-Gas Atmosphere

The CMP process may be carried out in an ultra-clean chamber in an air atmosphere. Due to the strong chemical inertness of 4H-SiC, researchers proposed to change the gas atmosphere to increase the rate of oxidation by placing the polishing device in a closed chamber and changing its gas atmosphere by delivering certain gas inward (**Figure 8**).[43] By changing the gas atmosphere of CMP from air to O_2, the MRR of 4H-SiC wafers increased from 35 to 60 nm h^{-1}.[44] The MRR during the CMP of 4H-SiC wafers significantly increased from 25 to 200 nm h^{-1} by adding bubbles of ozone gas to the polishing slurry.[45] In these studies, the MRR of the CMP of 4H-SiC wafers in the atmosphere of O_2 or ozone is higher than that in an air environment. However, this method requires the polishing equipment to be sealed. The special gas atmosphere poses additional safety issue on the CMP of 4H-SiC wafers.

 © 2023 The Authors. Advanced Materials Interfaces published by Wiley-VCH GmbH

21967350, 2023, 13, Downloaded from https://onlinelibrary.wiley.com/doi/10.1002/admi.202202369 by Xiamen University, Wiley Online Library on [11/04/2024]. See the Terms and Conditions (https://onlinelibrary.wiley.com/terms-and-conditions) on Wiley Online Library for rules of use; OA articles are governed by the applicable Creative Commons License

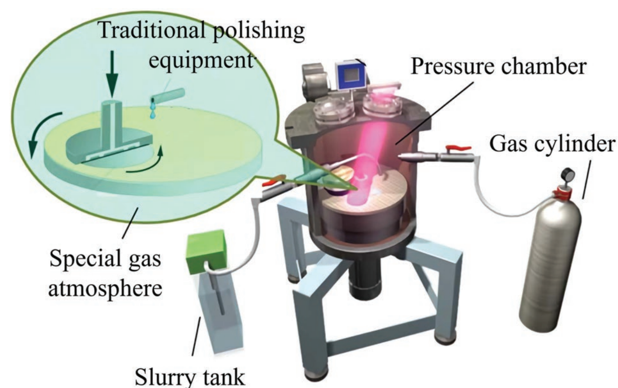

Figure 8. Schematic diagram of a special-gas-atmosphere improved CMP system, including auxiliary devices such as pressure chamber and gas cylinder. A gas cylinder is added to a closed CMP system, which guarantees the special-gas-atmosphere during CMP. Reproduced with permission.[43] Copyright 2012, IOP Publishing.

3.2.3. Pre-Processing

Pre-processing of 4H-SiC wafers includes chemical softening and activation (e.g., thermal oxidation and laser irradiation) before CMP.[46–55] With the pre-processing thermal oxidation at the temperature of 1100 °C for 10 h the formation rate of the oxide layer at the surface of a 4H-SiC wafer reaches 29 nm h^{-1}.[48] The laser irradiation method refers to the irradiation of a 4H-SiC wafer by an ultra-fast laser, including femtosecond laser, nanosecond laser, and picosecond laser.[56,57] Due to its high pulse frequency and high energy density, the ultra-fast laser introduces micro-pits or deep grooves at the surface of 4H-SiC wafers, which increases the effective contact area between the surface of 4H-SiC wafer and the polishing slurry during CMP. Hence, the efficiency of CMP may be improved. It was shown that the pretreatment of 6H-SiC wafer by a nanosecond fiber laser increased the MRR of CMP from 370 to 1700 nm h^{-1}.[57] By optimizing the laser processing parameters such as the laser power, repetition frequency, and scanning times through finite-element simulations and experimental research, the minimum width error of the laser-induced micro-grooves reached 2 µm and provided insights on the mechanism of the laser ablation of SiC.[53]

Among the pre-processing methods, the laser irradiation pretreatment can obtain a higher MRR without sacrificing the surface quality of a 4H-SiC wafer. This endows the laser irradiation pretreatment great potential in the improvement of the CMP of 4H-SiC wafers. As the diameter of 4H-SiC wafers is increasing to 200 mm, controlling the uniformity of laser ablation of the wafer without introducing new damages becomes the main challenge of the laser irradiation pre-processing. Moreover, the portability and controllability of the pre-processing approaches are common challenges for high-volume manufacturing of 4H-SiC wafers.

3.2.4. Photocatalysis-Assisted CMP

The photocatalysis-assisted CMP (PCMP) is based on the photosensitized oxidation reaction. As shown in **Figure 9**a, three factors, including the light source, photocatalyst, and electron capture agent, are involved in the photocatalysis reaction.[32] The ultraviolet (UV) or mercury lamp is used as the light source. The metal oxides such as nano-TiO_2 or nano-ZnO are selected as the photocatalyst. H_2O_2 or K_2FeO_4 is used as the electron capture agent.[58] Taking the slurry containing TiO_2 and H_2O_2 as an example, we show the reactions involved in a photocatalysis reaction as follows:[59]

$$TiO_2 + h\nu \rightarrow TiO_2 + h^+_{VB} + e^-_{CB} \quad (7)$$

$$e^-_{CB} + O_2 \rightarrow O_2^{\bullet -} \quad (8)$$

$$e^-_{CB} + H_2O_2 \rightarrow 2{}^\bullet OH \quad (9)$$

$$h^+_{VB} + H_2O \rightarrow {}^\bullet OH + H^+ \quad (10)$$

$$h^+_{VB} + OH^- \rightarrow {}^\bullet OH \quad (11)$$

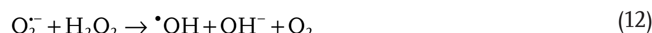
$$O_2^{\bullet -} + H_2O_2 \rightarrow {}^\bullet OH + OH^- + O_2 \quad (12)$$

During PCMP, electrons and holes are first excited into the conduction band (CB) and valance band (VB) of TiO_2 under UV-light illumination.[60] The photo-generated electrons and holes then diffuse to the surface of TiO_2. The electron capture agent

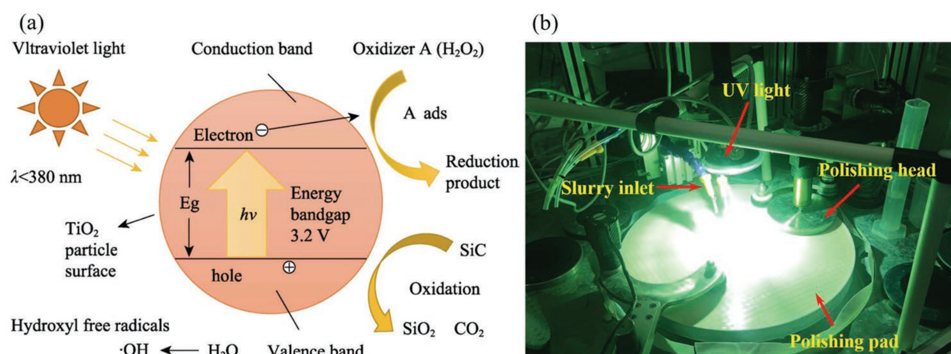

Figure 9. a) Schematic diagram showing the mechanism of photocatalytic oxidation of 4H-SiC. The synergistic effect of UV and TiO_2 increases the generation of $^\bullet$OH radicals in the polishing slurry, and then improves the oxidation efficiency of 4H-SiC during the CMP process. Reproduced with permission.[59] Copyright 2020, Elsevier. b) Image of the PCMP system with the UV lamp illuminated vertically above the polishing pad.

© 2023 The Authors. Advanced Materials Interfaces published by Wiley-VCH GmbH

of O_2 and H_2O_2 can effectively capture the electrons, generating reactive oxidizing species (ROS) of $O_2^{\bullet-}$ and $^{\bullet}OH$, respectively. The holes can be captured by H_2O and OH^-, forming highly ROS of $^{\bullet}OH$. Please note that the photo-generated electrons and holes at the surface of TiO_2 are not stable. The photocatalytic reaction ends with the recombination of photo-generated carriers. Combined with Equation (5), enhancing the efficiency of the ROS generation is beneficial to improving the oxidation of 4H-SiC and thus enhancing the efficiency of CMP.[61]

In 2017, the PCMP method was introduced into the polishing of 4H-SiC wafers.[62] 100 W UV LED was used as the light source. Nano-TiO_2 particles with an average diameter of 25 nm were used as the photocatalyst. H_2O_2 are the electron capture agent. The MRR for the CMP of 4H-SiC wafers significantly increased from 200 to 352.8 nm h^{-1}. The *Ra* of PCMP-treated 4H-SiC was as low as 0.0586 nm. The catalytic effect was further improved by directly irradiating the polishing slurry, rather than the polishing plate.[63] Most notably, a diamond-based slurry containing TiO_2 with an average diameter of 7 nm and cathilon dye was developed for polishing 4H-SiC wafers under mercury lamp illumination, which resulted in the MRR and *Ra* of 18.78 μm h^{-1} and 1.99 nm, respectively.[64]

The redox potential of the sulfate radical ($SO_4^{\bullet-}$) (2.60–3.10 V) is higher than that of $^{\bullet}OH$ (1.90–2.70 V). The lifetime of $SO_4^{\bullet-}$ (30–40 μs) is higher than that of $^{\bullet}OH$ (≤1 μs).[65,66] Hence, the sulfate radical-based advanced oxidation processes (SR-AOPs) are promising to improve the efficiency of PCMP. By activating potassium persulfate ($K_2S_2O_8$) with the synergy of UV and TiO_2, the MRR and surface roughness (*Sq* [the root mean square deviation]) were 608 nm h^{-1} and 0.521 nm, respectively. The mechanism for the enhancement of the CMP efficiency based on SR-AOPs is summarized as:[32]

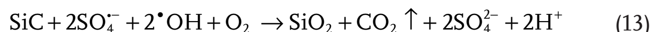

$$SiC + 2SO_4^{\bullet-} + 2^{\bullet}OH + O_2 \rightarrow SiO_2 + CO_2\uparrow + 2SO_4^{2-} + 2H^+ \quad (13)$$

The PCMP method can improve MRR and maintain excellent surface quality.[58,59,64,67–70] Furthermore, PCMP only requires adding a UV light source, which requires neither structural modifications to existing CMP equipments nor additional complex equipments. Therefore, PCMP holds great promise for the use with existing CMP procedures. However, there exist several challenges. Firstly, the dispersity of photocatalysts in the slurry needs to be guaranteed. PCMP processes often use nano-particles as photocatalysts. But such nanoparticles are highly prone to agglomeration in the aqueous phase, leading to decrease in the photocatalytic efficiency. This requires further improvement of the dispersion stability of the photocatalytic nanoparticles in the slurry. Secondly, the performance degradation of polishing pads undergoing prolonged UV illumination needs to be solved. Finally, the heat generated by prolonged UV-lamp illumination may affect the performance of the polishing slurry, which requires further investigation.

3.2.5. Catalyst-Referred Etching

The catalyst-referred etching (CARE) method belongs to an abrasive-free planarization method. As shown in **Figure 10**, the CARE device consists of a polishing pad with catalytic properties and a wafer holder, which are immersed in an etchant-filled vessel.[71,72] The CARE method accelerates the etching of 4H-SiC by the etchant through the catalytic effect of Pt metal films. The MRR and *Ra* obtained by the CARE method using hydrofluoric acids (HF) as the etchant were 100–200 nm h^{-1} and 0.1 nm, respectively.[73] A comparative experiment was performed by adding KF and NH_4F to the etchant. The results showed that MRR correlated positively with $[HF]\times([F^-]+[HF_2^-])$, suggesting that HF molecules and fluorine (F^- and HF_2^-) ions were the active components during the CARE process.[74]

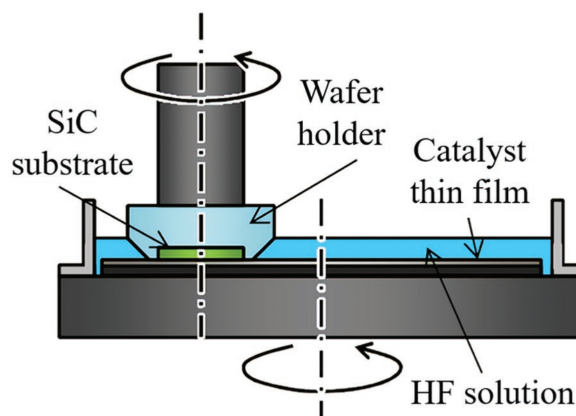

Figure 10. Schematic diagram of the CMP system equipped with CARE, which is composed of the polishing pad with catalytic properties, etching solution and wafer holder. Reproduced with permission.[71] Copyright 2014, Transtec Publications.

In general, the highly ordered surfaces of 4H-SiC wafers can be observed after polishing using the CARE method. But the toxicity of HF cannot be ignored. Therefore, replacing HF with other environmentally friendly etchants should be considered in the future development of the CARE method.

3.3. Mechanical-Improvement Approaches

3.3.1. Single-Abrasive Slurry

The polishing slurry usually contains only one kind of abrasives. **Table 1** lists the Mohs hardness and Knoop hardness of common abrasive particles.[75] Various abrasives, such as cerium dioxide (CeO_2), alumina (Al_2O_3), boron carbide (B_4C), SiC, and nano-diamonds, have been employed to enhance mechanical action during the CMP of 4H-SiC wafers. In addition to the SiO_2 abrasives described above, Al_2O_3 abrasives are also widely used for polishing 4H-SiC wafers given their hardness between that of 4H-SiC and SiO_2.[76–80] After decades of development, the MRR and *Ra* of polishing 4H-SiC based on

Table 1. Comparison of hardness of abrasive particles commonly used in CMP.[73]

Abrasive type	Diamond	B_4C	SiC	Al_2O_3	SiO_2	CeO_2
Mohs hardness	10	9.4	9.2	9	7	6

© 2023 The Authors. Advanced Materials Interfaces published by Wiley-VCH GmbH

21967350, 2023, 13, Downloaded from https://onlinelibrary.wiley.com/doi/10.1002/admi.202202369 by Xiamen University, Wiley Online Library on [11/04/2024]. See the Terms and Conditions (https://onlinelibrary.wiley.com/terms-and-conditions) on Wiley Online Library for rules of use; OA articles are governed by the applicable Creative Commons License

the single Al_2O_3 abrasive slurry have reached 0.98 μm h^{-1} and 0.235 nm, respectively.[80]

CeO_2 abrasives were initially used in the CMP of Si_3N_4 or SiO_2 materials. Although the hardness of CeO_2 is lower than that of SiO_2, the surface of CeO_2 particles tends to form oxygen vacancies, which enables Ce ions to achieve an oxidation state (Ce^{3+}/Ce^{4+}) transition.[81] This valence change reaction imparts CeO_2 particles with a unique chemical activity, enhancing the removal of oxidized 4H-SiC. Additionally, the Si—O—Ce chemical tooth can increase the friction coefficient between the slurry and the 4H-SiC wafer during the CMP. Therefore, higher MRR (1089 nm h^{-1}) and lower *Ra* (0.11 nm) were obtained by using CeO_2 as the abrasive and $KMnO_4$ as the oxidizing agent.[35] According to Yamamura et al.'s investigations, the effect of mechanical friction prevails over that of the chemical activity of CeO_2 abrasives during the CMP.[82]

In particular, researchers have also attempted to polish SiC with nano-scale diamond abrasives to achieve elastic interaction and high MRR of 4H-SiC wafers, due to the superior hardness of the diamond material.[83–86] However, the higher MRR is usually achieved by sacrificing the surface quality, giving rise to the mechanical polishing of 4H-SiC wafers. Huang et al.'s recent work showed that the MRR increased with the increase of the size of diamond particles (from 100 nm to 1 μm), while the surface quality deteriorated.[86] When the diamond particle were 1 μm large, the MRR and *Ra* were 1.1 μm h^{-1} and 1.2 nm, respectively.

Since it is difficult to obtain high MRR by using SiO_2-based slurries, researchers have tried to use Al_2O_3 or diamond particles with higher hardness as abrasive particles. It has been found that a single nano-diamond slurry introduces new scratches or subsurface damage at the wafer surface, although it renders extremely high MRR. In this context Al_2O_3-based polishing slurry with hardness higher than SiO_2 but lower than 4H-SiC becomes an ideal choice. The preparation of alumina suspensions has been a research hotspot in the field of powder processing.[87] Especially, when considering the application in the CMP field, we should be aware that the dispersion stability is a more serious problem under the combined action of strong acid and strong oxidant.[88] In addition to hard abrasive particles, a single CeO_2 slurry with stronger chemical activity but lower hardness has also been used to polish 4H-SiC, which can achieve higher MRR (>1 μm h^{-1}) without sacrificing surface quality. However, CeO_2 and Si atoms will combine to form Si—O—Ce chemical teeth with strong binding energy, which presents challenges to the post-cleaning technology of residual CeO_2 particles at the surface of 4H-SiC wafer after the CMP.[89,90] In the meantime, the preparation of the rare-earth material of CeO_2 requires complex purification processes, giving rise to the high price of commercial CeO_2-based polishing slurries.

3.3.2. Mixed-Abrasive Slurry

A mixed-abrasive slurry (MAS) contains two or more types of solid-phase abrasives,[91] including ZrO_2/SiO_2, nano-diamond/SiO_2, polymeric magnesium iron aluminum zinc silicate/SiO_2, SiO_2/CeO_2, and ZrP/Al_2O_3.[92–96] Compared with the single-abrasive slurry, a MAS exhibits better CMP performance. It has been found that adding 10 wt% diamond abrasives to SiO_2 slurry could increase the MRR from 60 to 600 nm h^{-1} and reduce the Ra from 68.3 to 0.55 nm.[97,98] The CMP performance (MRR: 920 nm h^{-1}, *Ra*: 0.52 nm) was further improved after adding 10 vol% NaClO to the preceding MAS. It was proposed that the added diamond particles not only enhanced the grinding action of the slurry, but also increased the local pressure at the 6H-SiC wafer surface. Hence, the tribo-chemistry reaction at the SiC/slurry interface was promoted.

Recently, a novel MAS system based on graphene oxide (GO)-based aqueous nanosuspensions was developed to polish 4H-SiC wafers.[86] As shown in **Figure 11**a,b, monocrystalline diamond particles (particle size: 1 μm) and multi-layered GO nanosheets were mixed into a slurry with a mass ratio of 1:8. The MAS resulted in the MRR of 0.8–0.9 μm h^{-1} and the surface roughness is 0.6–0.7 nm. The synergistic mechanism is proposed in Figure 11c. In general, GO nanosheets were reduced by friction action during the CMP. The generated ˙OH and •COOH radicals promoted the oxidation reaction at the 4H-SiC surface. Meanwhile, the reduced GO nanosheets could be deposited on the surface of SiC, forming a lubricating film and reducing the formation of scratches by diamond abrasives. In addition, Wang et al. designed a MAS system containing ZrO_2 particles with the size of 50–100 nm and Al_2O_3 particles with the size of 300–400 nm by high-energy ball milling (**Figure 12**a).[99] The resulting MRR and *Ra* were 694 nm h^{-1} and 0.489 nm, respectively. As shown in Figure 12b, ZrO_2 with photocatalytic activity could enhance the chemical action of the slurry, and the small-sized ZrO_2 particles and large-sized Al_2O_3 particles played a mechanically complementary role in the material removal process.

In summary, MAS technologies have potential applications in the CMP of 4H-SiC wafers.[21,100] But technical issues including the MAS preparation and storage and the post-CMP cleaning need to be further investigated.

3.3.3. Core–Shell Abrasive

As shown in **Figure 13**, a hard particle is commonly used as the core material, which is coated with the shell material with low hardness or better chemical activity.[101] It is promising that the resulting core–shell particle synthesized with a specific process has the advantages of both the core and shell materials. Typical core–shell abrasives and their CMP performance for SiC wafers are summarized in **Table 2**.[101–106] It is clear that the structures of core–shell abrasives are designed for specific polishing processes. Especially, in the PCMP process, TiO_2 is used as the shell material due to its photocatalytic activity. In the electrochemical mechanical polishing (ECMP) process, CeO_2 is selected as the shell material because of valence change. It is interesting that the MRR of ≈2.3 μm h^{-1} and *Ra* of 0.449 nm were achieved using polystyrene/CeO_2 core–shell abrasives in the ECMP.[105] When polyurethane or polystyrene is used as the core particle, the abrasive particles have a better elastic effect, making the material removal mechanism shift from the ploughing regime to the adhering regime. This is conducive to obtaining a good surface quality after polishing.

© 2023 The Authors. Advanced Materials Interfaces published by Wiley-VCH GmbH

21967350, 2023, 13, Downloaded from https://onlinelibrary.wiley.com/doi/10.1002/admi.202202369 by Xiamen University, Wiley Online Library on [11/04/2024]. See the Terms and Conditions (https://onlinelibrary.wiley.com/terms-and-conditions) on Wiley Online Library for rules of use; OA articles are governed by the applicable Creative Commons License

21967350, 2023, 13, Downloaded from https://onlinelibrary.wiley.com/doi/10.1002/admi.202202369 by Xiamen University, Wiley Online Library on [11/04/2024]. See the Terms and Conditions (https://onlinelibrary.wiley.com/terms-and-conditions) on Wiley Online Library for rules of use; OA articles are governed by the applicable Creative Commons License

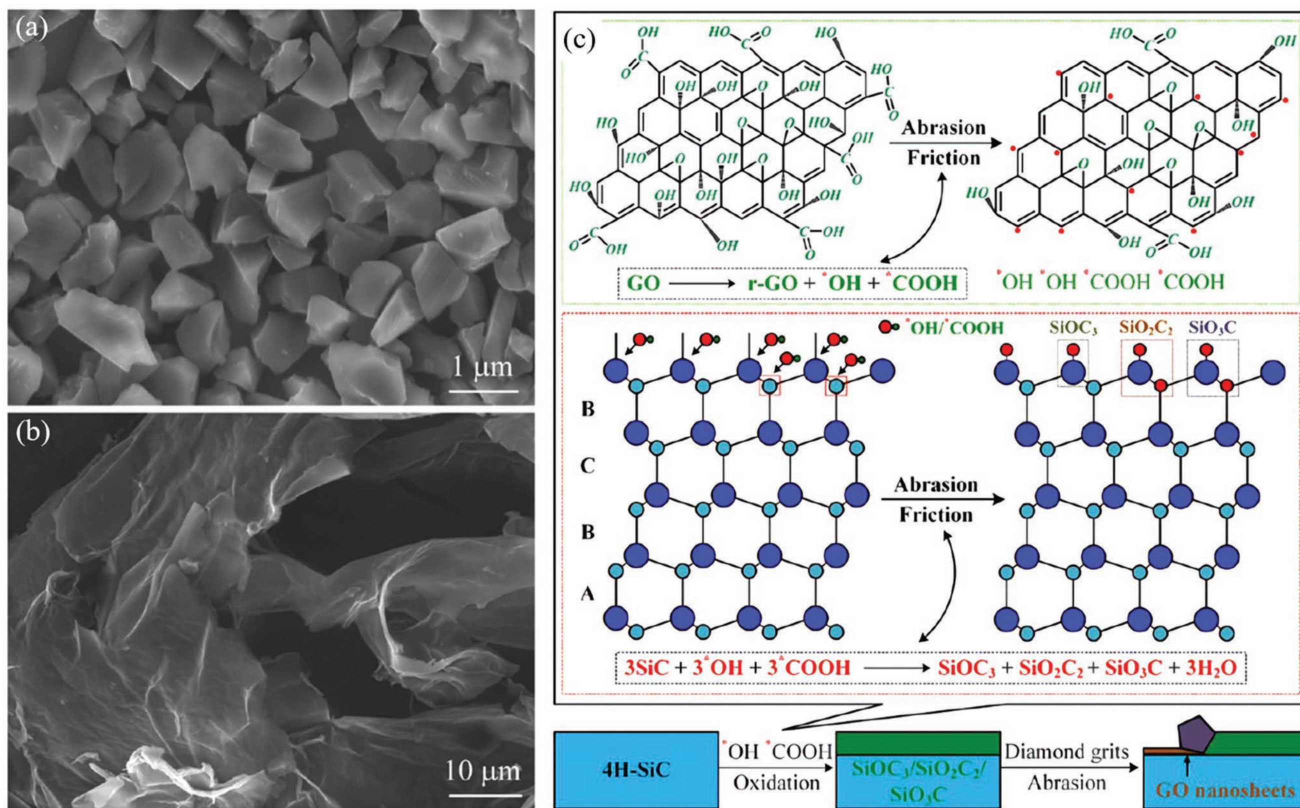

Figure 11. Mixed-abrasive slurry containing diamond particles and graphene oxide nanosheets: a) SEM image of diamond particles, b) SEM image of graphene oxide nanosheets with oxidation degree of 45%, and c) schematic diagram of improvement mechanism of mixed abrasive slurry, in which the graphene oxide nanosheet promotes free radical generation and reduces diamond grinding induced scratches. Reproduced with permission.[86] Copyright 2021, Elsevier.

Comprehensive literature analysis shows that designing corresponding core–shell abrasive particles for a specific polishing process may enhance the efficiency of CMP of 4H-SiC wafers. However, current core–shell abrasive particles have the shortcomings of a complicated preparation process and low uniformity of shell coating, which makes the method difficult to do under the industrial scale.[107]

3.3.4. Fixed or Semi-Fixed Abrasive

As shown in **Figure 14**, fixed-abrasive polishing (FAP) can improve the utilization efficiency of the abrasives by fixing the abrasives on the polishing pad through hot-pressing consolidation, UV curing, or sol–gel technology.[108] The resin-bonded ultra-fine diamond abrasive polishing pad was prepared

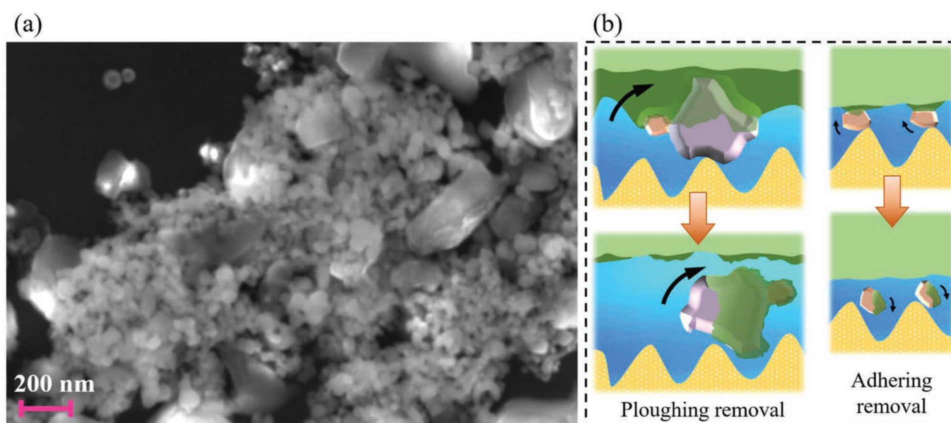

Figure 12. a) SEM image of mixed-abrasive slurry containing alumina particles (300–500 nm) and zirconium dioxide particles (50–80 nm). b) Synergistic mechanism of mixed abrasive particles during CMP, because the small-sized ZrO_2 particles and large-sized Al_2O_3 particles play a mechanically complementary role in the material-removal process. Reproduced with permission.[99] Copyright 2022, Elsevier.

 © 2023 The Authors. Advanced Materials Interfaces published by Wiley-VCH GmbH

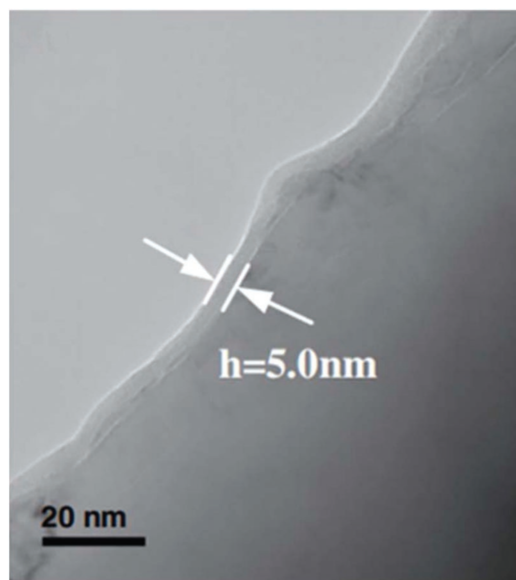

Figure 13. Transmission electron microscopy image of SiO_2 coating on diamond abrasives, with the thickness of the SiO_2 coating being 5 nm. The dark area in the lower right corner of the figure represents the diamond particles, and the light area near the diagonal area of the picture represents the SiO_2 film. Reproduced with permission.[101] Copyright 2017, Elsevier.

by electrophoretic co-deposition process, with which the Ra dropped from 90.3 to 4.3 nm after polishing the Si-face of SiC wafers in 1 h.[109] In another study, the MRR increased from 450 nm h^{-1} to 1.08 µm h^{-1} when replacing the polyurethane pad with a fixed-diamond-abrasive pad.[110] The FAP process can also achieve chemical efficiency enhancement during the CMP of SiC wafers by immobilizing various materials. A polishing pad with fixed Fe powder and Al_2O_3 abrasives was designed, and then used together with an abrasive-free polishing slurry containing 20 wt% H_2O_2 to polish 4H-SiC wafers, leading to an MRR of 740 nm h^{-1} and Sa (the mean difference in height from the mean plane) of 0.159 nm.[111]

Furthermore, semi-fixed abrasive polishing (Semi-FAP) has been proposed, in which the abrasive can be moved up and down within a limited range of the pad surface by the action of soft binding agents, such as unsaturated resins and sodium alginate salts.[109,112,113] Compared with the FAP process, it is easier for Semi-FAP to obtain an atomically smooth surface of a 6H-SiC wafer.[114]

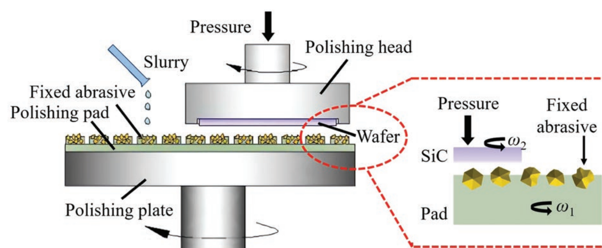

Figure 14. Schematic diagram of the fixed abrasive polishing, where the abrasive particles are fixed on the surface of the polishing pad. Reproduced with permission.[108] Copyright 2022, Springer Nature.

To date, FAP and Semi-FAP have been shown to significantly improve the MRR of 4H-SiC materials, while simultaneously solving the stability problem of free abrasive particles in the slurry. However, the fixed diamond particles generate fragments due to the abrasion of 4H-SiC wafers during the CMP process. These fragments can introduce severe scratches and subsurface damage if not removed from the polishing pad in time.

3.4. Chemical–Mechanical Synergistic Improvement Approaches

3.4.1. Electro-Chemical Mechanical Polishing

Conventional CMP technologies use chemical reagents such as H_2O_2, $KMnO_4$, and $K_2S_2O_8$ as oxidizing agents. An alternative strategy to improve the efficiency of CMP relies on the introduction of anodization based on electrochemical reactions, which is referred to as ECMP.[105,106,115–121] A common setup for the ECMP is schematically displayed in **Figure 15**.[117] A constant voltage or current is applied to the conductive path formed by the electrolyte (i.e., slurry), 4H-SiC wafer and copper plate by using a potentiostat. In the applied electric field the surface of the 4H-SiC wafer (i.e., anode) rapidly reacts to form an oxide layer. Then the oxide layer is removed by abrasives in the electrolyte. It can be seen from **Figure 16** that the transition oxide SiO_xC_y was rapidly formed on the surface of the 4H-SiC wafer after 2 min polishing. This softened layer is mechanically removed by the abrasive particles in the slurry. Subsequently,

Table 2. Comparison of core–shell abrasive applications in the CMP of SiC wafers.

Structure of core–shell abrasive				CMP performance		Notes
Core		Shell		MRR [µm h^{-1}]	*Ra* [nm]	
Material	Diameter [µm]	Material	Thickness [nm]			
Diamond	1	SiO_2	<1	0.066	3.700	CMP[101]
Diamond	0.6	TiO_2	<5	0.111	0.915	PCMP[102]
Polystyrene	160	CeO_2–TiO_2	20	0.122	0.497	PCMP[103]
Polyurethane	Unspecified	CeO_2	Unspecified	3.0–4.0	6.610	ECMP[104]
Polystyrene	Unspecified	CeO_2	Unspecified	≈2.300	0.449	ECMP[105]
Polystyrene	200	CeO_2	8.5–27.5	Unspecified	2.388	ECMP[106]

 © 2023 The Authors. Advanced Materials Interfaces published by Wiley-VCH GmbH

21967350, 2023, 13, Downloaded from https://onlinelibrary.wiley.com/doi/10.1002/admi.202202369 by Xiamen University, Wiley Online Library on [11/04/2024]. See the Terms and Conditions (https://onlinelibrary.wiley.com/terms-and-conditions) on Wiley Online Library for rules of use; OA articles are governed by the applicable Creative Commons License

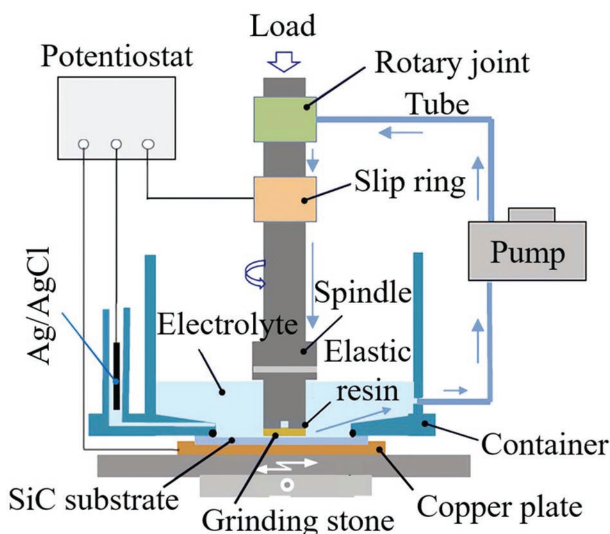

Figure 15. Schematic diagram of electro-chemical mechanical polishing device, where the SiC wafer, electrolyte, and copper plate form an electronically conductive path. Reproduced with permission.[117] Copyright 2019, Elsevier.

the new surface exposed on the wafer surface is oxidized again. Ultimately, the dynamic cycle of "oxidation-removal" results in the planarization of 4H-SiC wafers. Since the occurrence of the cycle of "oxidation-removal" is dynamic, the appearance and removal of SiC_xO_y is also transient. Therefore, this method can effectively improve the oxidation rate of SiC material.[122] The type of electrolyte has an important influence on the ECMP results. Using KNO_3 and SiO_2 as the electrolyte, and a continuously applied constant current of 20 mA cm^{-2}, Li et al. obtained that the MRR and Sq were 400–500 nm h^{-1} and 10.52 nm, respectively.[123] By contrast, if NaCl solution was used as the electrolyte, the most outstanding MRR (*Sq*) was 23 µm h^{-1} (1.352 nm) at the current of 10 mA cm^{-2}.[117]

3.4.2. Plasma-Assisted Polishing

Plasma-assisted polishing (PAP) is a novel polishing technology combining the irradiation of atmospheric pressure plasma and soft abrasive polishing.[124–129] **Figure 17**a shows that PAP requires the addition of a plasma-assisted module consisting of a radio-frequency electric power, a helium-based water vapor generator, and an ultrapure water bubbling machine to the CMP equipment.[130] In 2010, some researchers employed high-frequency electricity to produce plasma from water vapor containing helium, which was then delivered to the wafer surface by the bubbling method.[131] The surface of a 4H-SiC wafer was oxidized under the plasma. The resulting oxide layer was then mechanically removed by CeO_2 abrasives. The hardness of the 4H-SiC surface was reduced from 37.38 to 4.53 GPa. The root mean squared roughness of the 4H-SiC wafer after the PAP was 0.28 nm. Further work indicated that the presence of $\cdot$OH played a dominant role in the oxidation of the 4H-SiC wafer.[132] Figure 17b shows the cross-sectional transmission electron microscope image of a 4H-SiC wafer after 1 h of plasma irradiation. The middle layer was an 80 nm thick oxide layer.[133] It is interesting that the SiO_2/SiC boundary was atomically smooth. Although the formation of the atomically smooth boundary was not fully understood, it was considered to be critical to the planarization of the PAP.

3.4.3. Other Synergistic Approaches

The improvement of the performance of CMP results from the synergy of the chemical oxidation and mechanical removal process. When the mechanical removal is weaker than the chemical oxidation, the oxide layer at the surface of 4H-SiC wafers cannot be timely removed. This hinders the oxidation and ultimately lowers the MRR. On the contrary, if the mechanical removal is too strong, scratches may be introduced at the surface of a 4H-SiC wafer during CMP. Therefore, researchers have investigated synergistic efficiency enhancement to achieve a balance between mechanical and chemical interactions. As summarized in **Table 3**, several efficiency-enhancing methods concerning Fenton-like reaction, core/shell abrasive particles, FAP, PCMP, and MAS have been combined to form a hybrid polishing system.[43,54,99,102,105,111,134–139] It can be seen that the synergistic approaches including Fenton-like reaction combined with FAP, ECMP combined with core–shell abrasives, and PCMP combined with MAS help simultaneously achieve high MRR and good surface quality ($Ra < 0.5$ nm).

Since the efficiency of CMP is limited by the oxidation of 4H-SiC, researchers have developed synergistic oxidation approaches such as the plasma-assisted electrochemical oxidation, the ultrasonic-assisted electrochemical oxidation, and the electro-assisted photocatalysis oxidation.[140–143] Among these approaches, the highest oxidation rate of SiC reaches 57.1 nm min^{-1} when the anodic oxidation is employed. This provides a clue for the future improvement of the CMP for 4H-SiC wafers.[144]

The synergistic enhancement methods are capable of balancing the chemical and mechanical interactions during CMP. They are the most attractive for the improvement of the CMP of 4H-SiC wafers. In the meantime, we should bear in mind that reducing the cost of CMP is one of the most important issues for the commercialization of synergistic enhancement methods.

4. Conclusions and Prospects

In summary, we have reviewed the CMP of 4H-SiC wafers. Although CMP has achieved great success on the processing of 4H-SiC wafers,[145,146] chemical, mechanical, and chemical–mechanical synergistic improvement approaches have been proposed to enhance the MRR of CMP, and improve the surface quality of 4H-SiC wafers.

For chemical improvement approaches, the Fenton-like reaction may improve the efficiency of CMP with low cost. But residual Fe ions after CMP pose a challenge for post-CMP cleaning. For the emerging PCMP, the long-term stability of the photocatalyst in the slurry is an important issue. Furthermore, the temperature fluctuation induced by

 © 2023 The Authors. Advanced Materials Interfaces published by Wiley-VCH GmbH

21967350, 2023, 13, Downloaded from https://onlinelibrary.wiley.com/doi/10.1002/admi.202202369 by Xiamen University, Wiley Online Library on [11/04/2024]. See the Terms and Conditions (https://onlinelibrary.wiley.com/terms-and-conditions) on Wiley Online Library for rules of use; OA articles are governed by the applicable Creative Commons License

21967350, 2023, 13, Downloaded from https://onlinelibrary.wiley.com/doi/10.1002/admi.202202369 by Xiamen University, Wiley Online Library on [11/04/2024]. See the Terms and Conditions (https://onlinelibrary.wiley.com/terms-and-conditions) on Wiley Online Library for rules of use; OA articles are governed by the applicable Creative Commons License

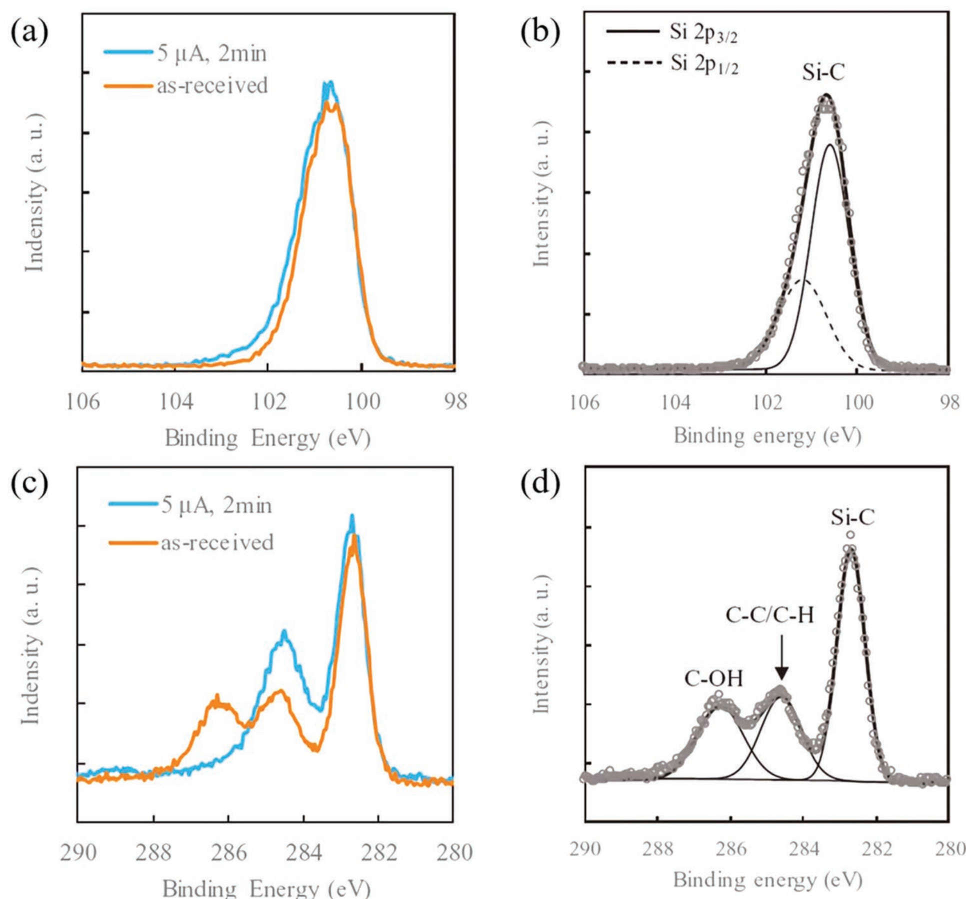

Figure 16. Comparison of XPS results after 2 min ECMP: (a) and (c) are the comparison of Si 2p and C 1s spectra before and after ECMP treatment; (b) and (d) correspond to Si 2p peak separation before and after treatment, respectively. Obvious oxide peaks of SiC_xO_y appeared in the XPS spectrum of 4H-SiC wafers after ECMP treatment. Reproduced with permission.[122] Copyright 2018, Elsevier.

long-time UV irradiation during PCMP should be monitored and controlled.

For mechanical improvement approaches, alumina- or ceria-based MAS and core–shell abrasive particles have been regarded as excellent components for novel polishing slurries. However, the dispersion stability of the nanoparticles needs to be optimized to increase the reliability and reproducibility of the high-volume fabrication of MAS or core–shell abrasive slurry.

For chemical–mechanical synergistic improvement approaches, a variety of new synergistic enhancement methods have been developed to improve the balance of chemical and mechanical interactions during the CMP of 4H-SiC wafers. It is suggested that future research could be extended to combine ECMP or PAP with traditional CMP methods to develop new processes for two-step polishing. In addition, understanding on the oxidation kinetics is crucial to

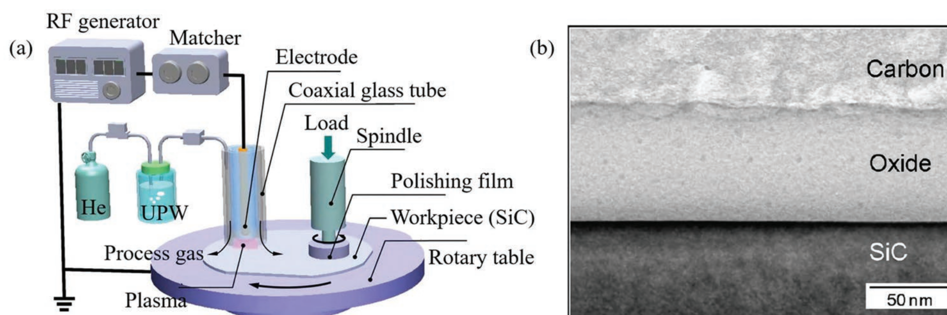

Figure 17. a) Schematic diagram of the PAP device, which consists of an independent external plasma generator and a conventional CMP system. Reproduced with permission.[130] Copyright 2012, Transtec Publications. b) Cross-sectional TEM image of the 4H-SiC wafer after PAP treatment for 1 h, showing a smooth SiC/SiO_2 boundary formed on the surface of SiC. Reproduced with permission.[133] Copyright 2013, Elsevier.

 © 2023 The Authors. Advanced Materials Interfaces published by Wiley-VCH GmbH

21967350, 2023, 13, Downloaded from https://onlinelibrary.wiley.com/doi/10.1002/admi.202202369 by Xiamen University, Wiley Online Library on [11/04/2024]. See the Terms and Conditions (https://onlinelibrary.wiley.com/terms-and-conditions) on Wiley Online Library for rules of use; OA articles are governed by the applicable Creative Commons License

Table 3. Comparison of representative CMP performance synergistic improvement approaches.

Ref.	Synergistic approaches	Components of slurry	CMP performance		Note
			MRR [μm h^{-1}]	Roughness [nm]	
Ho et al.[111]	a) Fenton-like b) FAP	H_2O_2/HCl	≈0.74	*Ra* = 0.159	1 wt% Fe and 3 wt% Al_2O_3-impregnated pad
Lu et al.[102]	a) Core–shell abrasives b) Semi-FAP c) PCMP	Abrasive-free	0.114	*Ra* = 0.915	TiO_2-coated diamond abrasives embedded in the pad
Zhou et al.[134]	a) PCMP b) FAP	SiO_2/H_2O_2	≈0.15	*Ra* = 0.0539	Modified TiO_2 incorporated pad
Gao et al.[105]	a) ECMP b) Core–shell abrasives	Polystyrene–CeO_2	≈2.3	*Ra* = 0.449	CeO_2 shells; Polystyrene cores
Tsai et al.[135]	a) PCMP b) MAS	TiO_2–graphene/ nano-diamond	3.8	*Sa* = 0.72	Diamond particle size: 50 nm
Ni et al.[136]	a) PCMP b) Fenton-like	Fe^{2+}/H_2O_2	0.092	*Ra* = 0.158	Fe^{2+} from $FeSO_4{\cdot}7H_2O$
He et al.[137]	a) PCMP b) ECMP c) Fenton-like	SiO_2/TiO_2	1.18	*Ra* = 0.61	
Yin et al.[43]	a) Special gas b) PCMP	SiO_2/TiO_2	≈0.07	*Ra* = 3.55	UV+O_2
Xie et al.[54]	a) Pre-processing b) Special gas	SiO_2	≈0.8	*Ra* = 32	Femtosecond laser pre-processing and pure O_2 atmosphere
Murata et al.[138]	a) ECMP b) FAP	CeO_2	1.8–9.2	*Sa* ≈ 0.68	*Sa* is 1 nm after ECMP
Liu et al.[139]	a) MAS b) Semi-FAP	Polyurethane microspheres–graphene oxide nanoplatelets–SiO_2	0.235	*Ra* ≈ 1	Chemically grafted ternary slurry
Wang et al.[99]	a) MAS b) PCMP	Al_2O_3/ZrO_2/H_2O_2	0.694	*Ra* = 0.489	

the improvement of PAP and ECMP. The composite polishing pad that associates photocatalysts with FAP is another key topic to discuss. The challenges of these approaches include the compatibility of compounding processes, technical fitting to customized wafer processing (e.g., different requirements of surface quality, thickness, and flatness), and fluctuation in processing cost.

To date, the emerging CMP efficiency enhancement technologies are still in the industrial validation stage of moving from the lab to the fab. Currently, PCMP and MAS technologies are showing potential in the industrial standard. In terms of leading on a research level, PAP and ECMP are considered to be more forward-looking.

Acknowledgements

This work is mainly supported by the Natural Science Foundation of China (Grant Nos. 62274143 and 62204216) , the "Pioneer" and "Leading Goose" R&D Program of Zhejiang (Grant No. 2022C01021) and the Leading Innovative and Entrepreneur Team Introduction Program of Hangzhou (TD2022012). Partial support is provided by the Natural Science Foundation of China for Innovative Research Group (Grant No. 61721005) and the Fundamental Research Funds for the Central Universities (Grant No. 226-2022-00200).

Conflict of Interest

The authors declare no conflict of interest.

Keywords

4H silicon carbide, chemical–mechanical polishing, material removal rate, surface roughness

Received: November 16, 2022
Revised: February 6, 2023
Published online: April 4, 2023

[1] X. She, A. Q. Huang, O. Lucia, B. Ozpineci, *IEEE Trans. Ind. Electron.* **2017**, *64*, 8193.
[2] C. Langpoklakpam, A. C. Liu, K. H. Chu, L. H. Hsu, W. C. Lee, S. C. Chen, C. W. Sun, M. H. Shih, K. Y. Lee, H. C. Kuo, *Crystals* **2022**, *12*, 245.
[3] X. Wang, Y. Zhong, H. Pu, J. Hu, X. Feng, G. Yang, *J. Semicond.* **2021**, *42*, 112802.
[4] S. Buschhorn, K. Vogel, in *PCIM Europe 2014; Int. Exhibition and Conf. for Power Electronics, Intelligent Motion, Renewable Energy and Energy Management*, Verband Deutscher Elektrotechniker, Nuremberg, Germany **2014**, pp. 1–7.

 © 2023 The Authors. Advanced Materials Interfaces published by Wiley-VCH GmbH

[5] T. Sugiura, A. Tanida, K. Tamura, *SAE Int. J. Altern. Powertrains* **2016**, *5*, 294.
[6] K. Sato, H. Kato, T. Fukushima, *IEEJ J. Ind. Appl.* **2021**, *10*, 402.
[7] T. Kimoto, J. A. Cooper, *Fundamentals of Silicon Carbide Technology: Growth, Characterization, Devices, and Applications*, 1st ed., Wiley & Sons, New York **2014**.
[8] T. Doi, *Int. J. Autom. Technol.* **2018**, *12*, 145.
[9] M. R. Marks, Z. Hassan, K. Y. Cheong, *Crit. Rev. Solid State Mater. Sci.* **2015**, *40*, 251.
[10] Y. G. Wang, L. C. Zhang, *Adv. Mater. Res.* **2010**, *126–128*, 429.
[11] Y. Zhou, G. S. Pan, X. L. Shi, H. Gong, G. H. Luo, Z. H. Gu, *Surf. Coat. Technol.* **2014**, *251*, 48.
[12] A. K. Agarwal, S. E. Saddow, *Advances in Silicon Carbide Processing and Applications*, 1st ed., Artech House, Boston **2004**.
[13] F. Bechstedt, P. Käckell, A. Zywietz, K. Karch, B. Adolph, K. Tenelsen, J. Furthmüller, *Phys. Status Solidi B* **1997**, *202*, 35.
[14] A. Naugarhiya, P. Wakhradkar, P. N. Kondekar, G. C. Patil, R. M. Patrikar, *J. Comput. Electron.* **2017**, *16*, 190.
[15] T. Kimoto, H. Matsunami, *J. Appl. Phys.* **1994**, *75*, 850.
[16] U. Forsberg, Ö. Danielsson, A. Henry, M. K. Linnarsson, E. Janzén, *J. Cryst. Growth* **2003**, *253*, 340.
[17] V. Šimonka, A. Toifl, A. Hössinger, S. Selberherr, J. Weinbub, *J. Appl. Phys.* **2018**, *123*, 235701.
[18] O. Kızılbey, O. Palamutçuoğullari, in 22nd Signal Processing and Communications Applications Conf. (SIU), IEEE, Piscataway, NJ **2014**, pp. 526–528.
[19] F. L. Guo, C. Shao, X. F. Chen, X. J. Xie, X. L. Yang, X. B. Hu, X. A. Xu, *Mater. Sci. Semicond. Process.* **2022**, *152*, 107124.
[20] Z. W. Zhong, *Mater. Manuf. Processes* **2020**, *35*, 1279.
[21] W. Zhai, B. Gao, *J. Harbin Inst. Technol.* **2018**, *50*, 1.
[22] Y. Takahashi, Polishing apparatus, *European Patent* EP0264572, **1987**.
[23] T.-Y. Kwon, M. Ramachandran, J.-G. Park, *Friction* **2013**, *1*, 279.
[24] T. Yin, T. Doi, S. Kurokawa, Z. Z. Zhou, K. P. Feng, *Int. J. Precis. Eng. Manuf.* **2018**, *19*, 1773.
[25] L. Zhou, V. Audurier, P. Pirouz, J. A. Powell, *J. Electrochem. Soc.* **1997**, *144*, 161.
[26] C. L. Neslen, W. C. Mitchel, R. L. Hengehold, *J. Electron. Mater.* **2001**, *30*, 1271.
[27] C. X.-f. L. I. Juan, M. A. De-ying, J. Shou-zhen, L. I. Xian-xiang, W. Li, D. Jie, H. U. Xiao-bo, X. U. Xian-gang, W. Ji-yang, J. Min-hua, *J. Funct. Mater.* **2006**, *37*, 70.
[28] G. S. Pan, Y. Zhou, G. H. Luo, X. L. Shi, C. L. Zou, H. Gong, *J. Mater. Sci.: Mater. Electron.* **2013**, *24*, 5040.
[29] X. L. Shi, G. S. Pan, Y. Zhou, Z. H. Gu, H. Gong, C. L. Zou, *Appl. Surf. Sci.* **2014**, *307*, 414.
[30] Y. Zhou, G. S. Pan, X. L. Shi, L. Xu, C. L. Zou, H. Gong, G. H. Luo, *Appl. Surf. Sci.* **2014**, *316*, 643.
[31] Y. Zhou, G. S. Pan, X. L. Shi, S. M. Zhang, H. Gong, G. H. Luo, *Tribol. Int.* **2015**, *87*, 145.
[32] W. T. Wang, B. G. Zhang, Y. H. Shi, T. D. Ma, J. K. Zhou, R. Wang, H. X. Wang, N. Y. Zeng, *J. Mater. Process. Technol.* **2021**, *295*, 117150.
[33] H. Aida, T. Doi, H. Takeda, H. Katakura, S. W. Kim, K. Koyama, T. Yamazaki, M. Uneda, *Curr. Appl. Phys.* **2012**, *12*, S41.
[34] W. Geng, G. Yang, X. Zhang, X. Zhang, Y. Wang, L. Song, P. Chen, Y. Zhang, X. Pi, D. Yang, R. Wang, *J. Semicond.* **2022**, *43*, 102801.
[35] G. M. Chen, Z. F. Ni, L. J. Xu, Q. Z. Li, Y. W. Zhao, *Appl. Surf. Sci.* **2015**, *359*, 664.
[36] M. Sato, K. Okuda, in *The 11th Int. Conf. on Precision Engineering (ICPE)*, Springer, New York **2007** p. 271.
[37] M. Pelaez, N. T. Nolan, S. C. Pillai, M. K. Seery, P. Falaras, A. G. Kontos, P. S. M. Dunlop, J. W. J. Hamilton, J. A. Byrne, K. O'Shea, M. H. Entezari, D. D. Dionysiou, *Appl. Catal., B* **2012**, *125*, 331.
[38] A. Kubota, K. Yagi, J. Murata, H. Yasui, S. Miyamoto, H. Hara, Y. Sano, K. Yamauchi, *J. Electron. Mater.* **2009**, *38*, 159.
[39] J. B. Lu, R. Chen, H. Z. Liang, Q. S. Yan, *Precis. Eng.* **2018**, *52*, 221.
[40] J. Deng, J. Pan, Q. Zhang, Q. Yan, J. Lu, *Surf. Interfaces* **2020**, *21*, 100730.
[41] J. Deng, Q. Zhang, J. Lu, Q. Yan, J. Pan, R. Chen, *Precis. Eng.* **2021**, *72*, 102.
[42] Q. Zhang, J. Pan, X. Zhang, J. Lu, Q. Yan, *Wear* **2021**, *472*, 203649.
[43] T. Yin, P. P. Zhao, T. Doi, S. Kurokawa, J. Y. Jiang, *ECS J. Solid State Sci. Technol.* **2021**, *10*, 6.
[44] O. Ohnishi, T. Doi, S. Kurokawa, T. Yamazaki, M. Uneda, T. Yin, I. Koshiyama, K. Ichikawa, H. Aida, *Jpn. J. Appl. Phys.* **2012**, *51*, 05EF05.
[45] M. Uneda, K. Fujii, *Precis. Eng.* **2020**, *64*, 91.
[46] H. Deng, K. Endo, K. Yamamura, *Appl. Phys. Lett.* **2013**, *103*, 111603.
[47] X. M. Shen, Y. F. Dai, H. Deng, C. L. Guan, K. Yamamura, *Opt. Express* **2013**, *21*, 14780.
[48] H. Deng, K. Endo, K. Yamamura, *Mater. Sci. Forum* **2014**, *778*, 587.
[49] H. Deng, K. Endo, K. Yamamura, *Appl. Phys. Lett.* **2014**, *104*, 101608.
[50] H. Deng, N. Liu, K. Endo, K. Yamamura, *Appl. Surf. Sci.* **2018**, *434*, 40.
[51] C. W. Wang, S. Kurokawa, T. Doi, J. L. Yuan, Y. Sano, H. Aida, K. H. Zhang, Q. F. Deng, *ECS J. Solid State Sci. Technol.* **2017**, *6*, P105.
[52] S. K. C. Wang, J. Yuan, L. Fan, H. Lu, Z. Wu, W. Yao, K. Zhang, Y. Zhang, T. Doi, *Int. J. Autom. Technol.* **2018**, *12*, 187.
[53] Z. Y. Zhai, C. Wei, Y. C. Zhang, Y. H. Cui, Q. R. Zeng, *Appl. Surf. Sci.* **2020**, *502*, 144131.
[54] X. Xie, Q. Peng, G. Chen, J. Li, J. Long, G. Pan, *Ceram. Int.* **2021**, *47*, 13322.
[55] Z. S. Zhang, H. Cai, D. Gan, W. J. Hu, J. W. Yang, X. Z. Liu, Y. L. Guo, L. W. Guo, W. J. Wang, X. L. Chen, *CrystEngComm* **2019**, *21*, 1200.
[56] B. Gao, D. Guo, X. Zhang, G. Chen, G. Pan, *ECS J. Solid State Sci. Technol.* **2021**, *10*, 044008.
[57] G. P. Chen, J. G. Li, J. Y. Long, H. M. Luo, Y. Zhou, X. Z. Xie, G. S. Pan, *Appl. Surf. Sci.* **2021**, *536*, 147963.
[58] Z. W. Yuan, Y. He, X. W. Sun, Q. Wen, *Mater. Manuf. Processes* **2018**, *33*, 1214.
[59] Q. S. Yan, X. Wang, Q. Xiong, J. B. Lu, B. T. Liao, *J. Cryst. Growth* **2020**, *531*, 125379.
[60] J. Wang, T. Q. Wang, G. S. Pan, X. C. Lu, *Appl. Surf. Sci.* **2016**, *361*, 18.
[61] A. Kubota, K. Kurihara, M. Touge, *Key Eng. Mater.* **2012**, *523–524*, 24.
[62] Z. Ye, Y. Zhou, L. Xu, G. Pan, *Nanotechnol. Precis. Eng.* **2017**, *15*, 342.
[63] L. Jiabin, X. Qiang, Y. Qiusheng, W. Xin, B. Shuiming, *Diamond Abrasives Eng.* **2019**, *03*, 29.
[64] T. Tanaka, M. Takizawa, A. Hata, *Int. J. Autom. Technol.* **2018**, *12*, 160.
[65] T. Olmez-Hanci, I. Arslan-Alaton, *Chem. Eng. J.* **2013**, *224*, 10.
[66] W. D. Oh, Z. L. Dong, T. T. Lim, *Appl. Catal., B* **2016**, *194*, 169.
[67] M. Mekata, M. Ota, K. Yamaguchi, E. Kai, *Int. J. Autom. Technol.* **2019**, *13*, 749.
[68] J. Lu, Q. Xiong, Q. Yan, X. Wang, K. Egashira, *Surf. Technol.* **2019**, *48*, 148.
[69] H. Yan, Y. Zewei, D. Zhenyun, Z. Youjun, *J. Harbin Inst. Technol.* **2019**, *51*, 115.
[70] T. Sakamoto, M. Touge, A. Kubota, *Prog. of Machining Technology Published by the 10th Int. Conf. on Progress of Machining Technology (ICPMT2012)* **2012**, p. 85.
[71] A. Isohashi, Y. Sano, S. Sadakuni, K. Yamauchi, *Mater. Sci. Forum* **2014**, *778–780*, 722.

© 2023 The Authors. Advanced Materials Interfaces published by Wiley-VCH GmbH

21967350, 2023, 13, Downloaded from https://onlinelibrary.wiley.com/doi/10.1002/admi.202202369 by Xiamen University, Wiley Online Library on [11/04/2024]. See the Terms and Conditions (https://onlinelibrary.wiley.com/terms-and-conditions) on Wiley Online Library for rules of use; OA articles are governed by the applicable Creative Commons License

[72] T. Okamoto, Y. Sano, K. Tachibana, B. V. Pho, K. Arima, K. Inagaki, K. Yagi, J. Murata, S. Sadakuni, H. Asano, A. Isohashi, K. Yamauchi, *Jpn. J. Appl. Phys.* **2012**, *51*, 046501.
[73] H. Hara, Y. Sano, H. Mimura, K. Arima, A. Kubota, K. Yagi, J. Murata, K. Yamauch, *J. Electron. Mater.* **2006**, *35*, L11.
[74] A. Isohashi, Y. Sano, T. Okamoto, K. Tachibana, K. Arima, K. Inagaki, K. Yagi, S. Sadakuni, Y. Morikawa, K. Yamauchi, *Mater. Sci. Forum* **2013**, *740*, 847.
[75] J. L. Yuan, B. H. Lü, X. Lin, L. B. Zhang, S. M. Ji, *J. Mater. Process. Technol.* **2002**, *129*, 171.
[76] S. Jianxiu, D. Jiaxi, L. Haina, L. Xinglong, *Proc. Eng.* **2011**, *24*, 441.
[77] S. Jianxiu, D. Jiaxi, M. Lijie, Z. Zhuqing, K. Renke, *J. Semicond.* **2012**, *33*, 106003.
[78] J. X. Su, J. X. Du, X. L. Liu, H. N. Liu, *Ultra-Precis. Mach. Technol.* **2012**, *497*, 250.
[79] C. Guo-mei, N. Zi-feng, Q. Shan-hua, L. Yuan-xiang, D. Chun-kuan, Z. Ling, X. Yi-cen, Z. Yong-wu, *J. Synth. Cryst.* **2019**, *01*, 155.
[80] Q. R. Liang, X. B. Hu, X. F. Chen, X. G. Xu, Y. M. Zong, X. J. Wang, *J. Synth. Cryst.* **2015**, *44*, 1741.
[81] J. Seo, J. Moon, J. H. Kim, K. Lee, J. Hwang, H. Yoon, D. K. Yi, U. Paik, *Appl. Surf. Sci.* **2016**, *389*, 311.
[82] H. Deng, K. Endo, K. Yamamura, *Sci. Rep.* **2015**, *5*, 8947.
[83] L. Yin, E. Y. J. Vancoille, K. Ramesh, H. Huang, *Int. J. Mach. Tool Manuf.* **2004**, *44*, 607.
[84] H. Y. Tam, H. B. Cheng, Y. W. Wang, *J. Mater. Process. Technol.* **2007**, *192*, 276.
[85] L. Yin, H. Huang, in Microelectronics: Design, Technology, and Packaging III, Vol. *6798*, SPIE, Bellingham, WA **2008**, p. 67981I.
[86] S. Q. Huang, X. L. Li, D. K. Mu, C. C. Cui, H. Huang, H. Huang, *Tribol. Int.* **2021**, *164*, 107241.
[87] F. Boutenel, G. Dusserre, A. Aimable, T. Chartier, T. Cutard, *Powder Technol.* **2021**, *393*, 630.
[88] Y. Qiusheng, X. Peijie, L. Jiabin, L. Huazhuo, *Semicond. Technol.* **2018**, *09*, 664.
[89] J. Seo, A. Gowda, S. V. Babu, *ECS J. Solid State Sci. Technol.* **2018**, *7*, 243.
[90] B. B. Wu, P. Wang, Y. J. Wang, X. P. Qu, B. M. Tan, S. Hamada, Y. Wada, H. Hiyama, *ECS J. Solid State Sci. Technol.* **2021**, *10*, 034010.
[91] A. Jindal, S. Hegde, S. V. Babu, *J. Electrochem. Soc.* **2003**, *150*, G314.
[92] S.-W. Park, Y.-J. Seo, W.-S. Lee, *Microelectron. Eng.* **2008**, *85*, 682.
[93] Y. C. Xu, J. Lu, X. P. Xu, *Appl. Surf. Sci.* **2016**, *389*, 713.
[94] T. X. Wang, H. Lei, Y. Dong, L. Xu, S. W. Dai, *J. Alloys Compd.* **2019**, *782*, 709.
[95] Y. Chen, C. Zuo, Z. Li, A. Chen, *J. Alloys Compd.* **2018**, *736*, 276.
[96] T. Li, H. Y. Sun, D. Q. Wang, J. T. Huang, D. D. Li, F. Lei, D. Z. Sun, *Appl. Surf. Sci.* **2021**, *537*, 147859.
[97] V. D. Heydemann, W. J. Everson, R. D. Gamble, D. W. Snyder, M. Skowronski, *Chemi-Mechanical Polishing of On-Axis Semi-Insulating SiC Substrates*, Trans Tech Publications Ltd. , Zurich-Uetikon **2004**.
[98] W. J. Everson, V. D. Heydemann, R. D. Gamble, D. W. Snyder, G. Goda, M. Skowronski, J. Grim, E. Berkman, J. M. Redwing, J. D. Acord, *Mater. Sci. Forum* **2006**, *527–529*, 1091.
[99] W. Wang, B. Zhang, Y. Shi, J. Zhou, R. Wang, N. Zeng, *Appl. Surf. Sci.* **2022**, *575*, 151676.
[100] M. Fan-ning, Z. Zhen-yu, G. Pei-li, M. Xiang-dong, L. Jian, *Surf. Technol.* **2019**, *07*, 1.
[101] J. Lu, Y. C. Xu, Y. H. Zhang, X. P. Xu, *Diamond Relat. Mater.* **2017**, *76*, 123.
[102] J. Lu, Y. G. Wang, Q. F. Luo, X. P. Xu, *Precis. Eng.* **2017**, *49*, 235.
[103] B. Gao, W. J. Zhai, Q. Zhai, M. Z. Zhang, *Appl. Surf. Sci.* **2019**, *484*, 534.
[104] J. Murata, K. Yodogawa, K. Ban, *Int. J. Mach. Tool Manuf.* **2017**, *114*, 1.
[105] B. Gao, W. J. Zhai, Q. Zhai, Y. L. Xia, C. Wang, K. X. Peng, *ECS J. Solid State Sci. Technol.* **2019**, *8*, 677.
[106] B. Gao, W. J. Zhai, Q. Zhai, Y. Q. Shi, *ECS J. Solid State Sci. Technol.* **2020**, *9*, 044005.
[107] X. Lai-jun, N. Zi-feng, C. Guo-mei, B. Ya-wen, Z. Yong-wu, *Bull. Chin. Ceram. Soc.* **2016**, *11*, 3855.
[108] Q. F. Luo, H. L. Wen, J. Lu, *Int. J. Adv. Manuf. Technol.* **2022**, *120*, 1415.
[109] J. Lu, Q. F. Luo, X. Y. Mao, X. P. Xu, Y. H. Wang, H. Guo, *Precis. Eng.* **2017**, *47*, 353.
[110] M. Y. Tsai, S. M. Wang, C. C. Tsai, T. S. Yeh, *Int. J. Adv. Manuf. Technol.* **2015**, *80*, 1511.
[111] J. K. Ho, C. Y. Huang, M. Y. Tsai, C. C. Tsai, *Appl. Sci.* **2016**, *6*, 89.
[112] J. Lu, Y. Li, X. P. Xu, *Proc. Inst. Mech. Eng., Part B* **2015**, *229*, 170.
[113] J. Lu, Q. F. Luo, X. P. Xu, H. Huang, F. Jiang, *Proc. Inst. Mech. Eng., Part B* **2019**, *233*, 69.
[114] Q. F. Luo, J. Lu, X. P. Xu, *Wear* **2016**, *350–351*, 99.
[115] H. Deng, K. Hosoya, Y. Imanishi, K. Endo, K. Yamamura, *Electrochem. Commun.* **2015**, *52*, 5.
[116] X. Yang, R. Y. Sun, Y. Ohkubo, K. Kawai, K. Arima, K. Endo, K. Yamamura, *Electrochim. Acta* **2018**, *271*, 666.
[117] X. Yang, X. Z. Yang, K. Kawai, K. Arima, K. Yamamura, *Int. J. Mach. Tool Manuf.* **2019**, *144*, 103431.
[118] X. Yang, X. Z. Yang, K. Kawai, K. Arima, K. Yamamura, *J. Manuf. Processes* **2021**, *70*, 350.
[119] B. Gao, W. J. Zhai, Q. Zhai, Y. Q. Shi, *ECS J. Solid State Sci. Technol.* **2021**, *10*, 044006.
[120] D. Jia-yun, P. Ji-sheng, Y. Qiu-sheng, *Surf. Technol.* **2020**, *04*, 64.
[121] J. Deng, J. Lu, Q. Yan, J. Pan, *J. Environ. Chem. Eng.* **2021**, *9*, 104954.
[122] X. Yang, Y. Ohkubo, K. Endo, K. Yamamura, *Proc. CIRP* **2018**, *68*, 746.
[123] C. H. Li, I. B. Bhat, R. J. Wang, J. Seiler, *J. Electron. Mater.* **2004**, *33*, 481.
[124] H. Deng, K. Endo, K. Yamamura, *Int. J. Mach. Tool Manuf.* **2017**, *115*, 38.
[125] H. Deng, M. Ueda, K. Yamamura, *Int. J. Adv. Manuf. Technol.* **2014**, *72*, 1.
[126] H. Deng, K. Monna, T. Tabata, K. Endo, K. Yamamura, *CIRP Ann.* **2014**, *63*, 529.
[127] H. Deng, K. Endo, K. Yamamura, *Procedia CIRP* **2014**, *13*, 203.
[128] H. Deng, K. Yamamura, *Mater. Sci. Forum* **2013**, *740*, 514.
[129] H. Deng, K. Yamamura, *Mater. Sci. Forum* **2013**, *740–742*, 435.
[130] H. Deng, M. Ueda, K. Yamamura, *Key. Eng. Mater.* **2012**, *516*, 186.
[131] K. Yamamura, T. Takiguchi, M. Ueda, A. N. Hattori, N. Zettsu, *Adv. Mater. Res.* **2010**, *126–128*, 423.
[132] H. Deng, T. Takiguchi, M. Ueda, A. N. Hattori, N. Zettsu, K. Yamamura, *Jpn. J. Appl. Phys.* **2011**, *50*, 08JG05.
[133] H. Deng, K. Yamamura, *CIRP Ann.* **2013**, *62*, 575.
[134] Y. Zhou, G. S. Pan, C. L. Zou, L. Wang, *ECS J. Solid State Sci. Technol.* **2017**, *6*, P603.
[135] M. Y. Tsai, Z. T. Hoo, *Int. J. Adv. Manuf. Technol.* **2019**, *105*, 1519.
[136] Z. Ping, C. Guo-mei, N. Zi-feng, X. Yong, D. Meng-jiao, W. Jian-me, L. Wei-min, Z. Hai-tao, *Surf. Technol.* **2020**, *07*, 253.
[137] Y. He, Z. W. Yuan, S. Y. Song, X. J. Gao, W. J. Deng, *Int. J. Precis. Eng. Manuf.* **2021**, *22*, 951.
[138] C. N. S. B. C. Zulkifle, K. Hayama, J. Murata, *Diamond Relat. Mater.* **2021**, *120*, 108700.
[139] H. K. Liu, C. C. A. Chen, P. C. Hsieh, *Int. J. Adv. Manuf. Technol.* **2022**, *120*, 7157.
[140] X. C. Yin, S. J. Li, G. L. Ma, Z. Jia, X. Liu, *RSC Adv.* **2021**, *11*, 27338.
[141] X. Z. Yang, X. Yang, K. Kawai, K. Arima, K. Yamamura, *Electrochem. Commun.* **2019**, *100*, 1.

© 2023 The Authors. Advanced Materials Interfaces published by Wiley-VCH GmbH

21967350, 2023, 13, Downloaded from https://onlinelibrary.wiley.com/doi/10.1002/admi.202202369 by Xiamen University, Wiley Online Library on [11/04/2024]. See the Terms and Conditions (https://onlinelibrary.wiley.com/terms-and-conditions) on Wiley Online Library for rules of use; OA articles are governed by the applicable Creative Commons License

ADVANCED MATERIALS INTERFACES
Open Access
www.advmatinterfaces.de

[142] Y. He, Z. W. Yuan, K. Cheng, Z. Y. Duan, W. Z. Zhao, *Proc. Inst. Mech. Eng., Part B* **2019**, *234*, 401.
[143] X. Z. Yang, X. Yang, H. Y. Gu, K. Kawai, K. Arima, K. Yamamura, *Ceram. Int.* **2022**, *48*, 7570.
[144] X. Yang, X. Yang, K. Kawai, K. Arima, K. Yamamura, *Appl. Surf. Sci.* **2021**, *562*, 150130.
[145] J. H. An, G. S. Lee, W. J. Lee, B. C. Shin, J. D. Seo, K. R. Ku, H. D. Seo, H. D. Jeong, *Mater. Sci. Forum* **2009**, *600*, 831.
[146] H. Yashiro, T. Fujimoto, N. Ohtani, T. Hoshino, M. Katsuno, T. Aigo, H. Tsuge, M. Nakabayashi, H. Hirano, K. Tatsumi, *Mater. Sci. Forum* **2009**, *600–603*, 819.

Wantang Wang received his Ph.D. from Hebei University of Technology in 2022. He is now a postdoctoral fellow at College of Electrical Engineering and Hangzhou Innovation Center at Zhejiang University. He has been engaged in research on chemical mechanical polishing (CMP) of semiconductor wafers, including the CMP mechanism, as well as the development and application of polishing slurries, polishing pads, and advanced polishing processes.

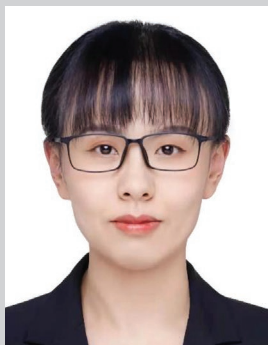

Rong Wang received her Ph.D. at the Zhejiang University in 2014. She is now a research fellow at the State Key Laboratory of Silicon and Advanced Semiconductor Materials & School of Materials Science and Engineering & Hangzhou Innovation Center at Zhejiang University. Her current research mainly concerns defects and impurities in wide-bandgap semiconductors.

Deren Yang received his Ph.D. in 1991 from Zhejiang University and then worked there. In 1990s, he worked in Japan, Germany, and Sweden for several years as a visiting researcher. He is now a member of the Chinese Academy of Science and the president of Ningbotech University in China. He has been engaged in the research of silicon materials used for microelectronic devices, solar cells, and nanodevices.

© 2023 The Authors. Advanced Materials Interfaces published by Wiley-VCH GmbH

21967350, 2023, 13, Downloaded from https://onlinelibrary.wiley.com/doi/10.1002/admi.202202369 by Xiamen University, Wiley Online Library on [11/04/2024]. See the Terms and Conditions (https://onlinelibrary.wiley.com/terms-and-conditions) on Wiley Online Library for rules of use; OA articles are governed by the applicable Creative Commons License

Xiaodong Pi received his Ph.D. degree at the University of Bath in 2004. He then carried out research at McMaster University and the University of Minnesota at Twin Cities. He joined Zhejiang University as an associate professor in 2008. He is now a professor at the State Key Laboratory of Silicon and Advanced Semiconductor Materials & School of Materials Science and Engineering & Hangzhou Innovation Center at Zhejiang University. His research interest is mainly in semiconductor materials and devices.

© 2023 The Authors. Advanced Materials Interfaces published by Wiley-VCH GmbH

21967350, 2023, 13, Downloaded from https://onlinelibrary.wiley.com/doi/10.1002/admi.202202369 by Xiamen University, Wiley Online Library on [11/04/2024]. See the Terms and Conditions (https://onlinelibrary.wiley.com/terms-and-conditions) on Wiley Online Library for rules of use; OA articles are governed by the applicable Creative Commons License